Article

Cell

Phase Separation of FUS Is Suppressed by Its Nuclear Import Receptor and Arginine Methylation

Graphical Abstract

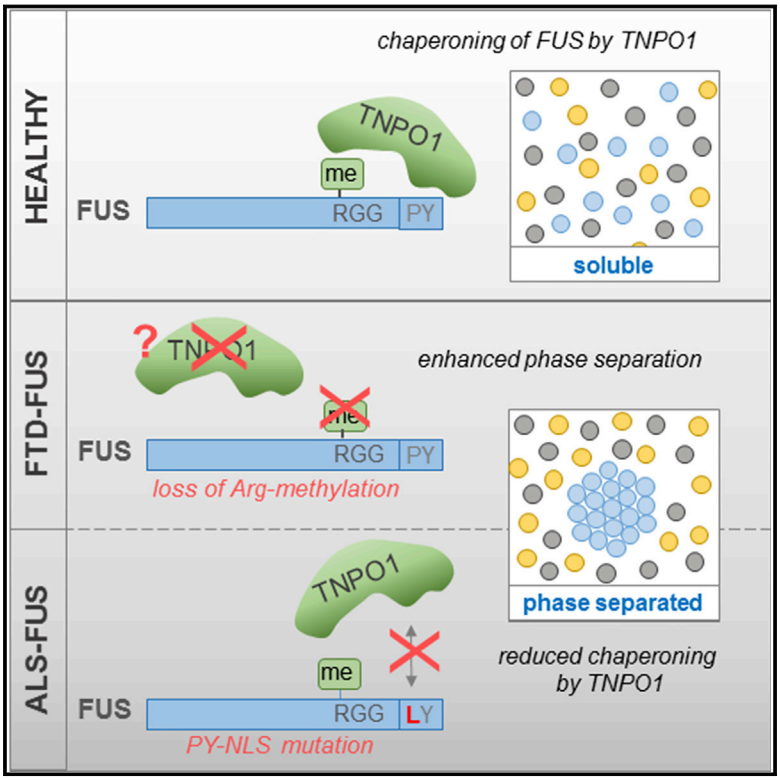

Highlights

- TNPO1 suppresses phase separation and stress granule (SG) association of FUS
- Disease-linked mutations in the NLS of FUS impair chaperoning by TNPO1
- Arginine residues in RGG/RG motifs are required for phase separation of FUS
- Loss of FUS arginine methylation promotes phase separation/SG association of FUS

Authors

Mario Hofweber, Saskia Hutten, Benjamin Bourgeois, ..., Dierk Niessing, Tobias Madl, Dorothee Dormann

Correspondence

dorothee.dormann@med.uni-muenchen.de

In Brief

Phase separation of FUS is regulated by both arginine methylation and binding to the nuclear import receptor Transportin/Karyopherin-β2, and this control can be compromised in the neurodegenerative diseases FTD and ALS.

Hofweber et al., 2018, Cell *173*, 706–719
April 19, 2018
https://doi.org/10.1016/j.cell.2018.03.004

CellPress

Cell

Article

Phase Separation of FUS Is Suppressed by Its Nuclear Import Receptor and Arginine Methylation

Mario Hofweber,[1,2,10] Saskia Hutten,[1,10] Benjamin Bourgeois,[3] Emil Spreitzer,[3] Annika Niedner-Boblenz,[1,4] Martina Schifferer,[5,6,7] Marc-David Ruepp,[8] Mikael Simons,[5,6,7] Dierk Niessing,[1,4,9] Tobias Madl,[3] and Dorothee Dormann[1,2,7,11,*]

[1]Biomedical Center (BMC), Ludwig-Maximilians University of Munich, 82152 Planegg-Martinsried, Germany
[2]Graduate School of Systemic Neurosciences (GSN), Ludwig-Maximilians University of Munich, 82152 Planegg-Martinsried, Germany
[3]Institute of Molecular Biology & Biochemistry, Center of Molecular Medicine, Medical University of Graz, 8010 Graz, Austria
[4]Institute of Structural Biology, Helmholtz Zentrum München, German Research Center for Environmental Health, 85763 Neuherberg, Germany
[5]Institute of Neuronal Cell Biology, Technical University of Munich, 80805 Munich, Germany
[6]German Center for Neurodegenerative Diseases (DZNE), 81377 Munich, Germany
[7]Munich Cluster for Systems Neurology (SyNergy); 81377 Munich, Germany
[8]Department of Chemistry and Biochemistry, University of Bern, 3012 Bern, Switzerland
[9]Institute of Pharmaceutical Biotechnology, Ulm University, 89081 Ulm, Germany
[10]These authors contributed equally
[11]Lead Contact
*Correspondence: dorothee.dormann@med.uni-muenchen.de
https://doi.org/10.1016/j.cell.2018.03.004

SUMMARY

Cytoplasmic FUS aggregates are a pathological hallmark in a subset of patients with frontotemporal dementia (FTD) or amyotrophic lateral sclerosis (ALS). A key step that is disrupted in these patients is nuclear import of FUS mediated by the import receptor Transportin/Karyopherin-β2. In ALS-FUS patients, this is caused by mutations in the nuclear localization signal (NLS) of FUS that weaken Transportin binding. In FTD-FUS patients, Transportin is aggregated, and post-translational arginine methylation, which regulates the FUS-Transportin interaction, is lost. Here, we show that Transportin and arginine methylation have a crucial function beyond nuclear import—namely to suppress RGG/RG-driven phase separation and stress granule association of FUS. ALS-associated FUS-NLS mutations weaken the chaperone activity of Transportin and loss of FUS arginine methylation, as seen in FTD-FUS, promote phase separation, and stress granule partitioning of FUS. Our findings reveal two regulatory mechanisms of liquid-phase homeostasis that are disrupted in FUS-associated neurodegeneration.

INTRODUCTION

Protein aggregates are a pathological hallmark of all neurodegenerative diseases and are thought to drive the process of neurodegeneration (Taylor et al., 2002). In ALS (amyotrophic lateral sclerosis) and FTD (frontotemporal dementia), the major aggregating proteins are two ubiquitously expressed RNA-binding proteins (RBPs) called TDP-43 (TAR DNA-binding protein of 43 kDa) and FUS (fused in sarcoma) (Neumann et al., 2006, 2009). TDP-43 and FUS are enriched in the cell nucleus, but in *post mortem* brains and spinal cords of ALS/FTD patients, they are often absent from the nucleus and are found in cytoplasmic aggregates in neuronal and sometimes glia cells (Mackenzie et al., 2010). RBP aggregation is thought to cause widespread disturbances in neuronal RNA metabolism and neurodegeneration by loss- and/or gain-of-function mechanisms (Ling et al., 2013). How cytosolic RBP aggregation arises and which cellular quality control mechanisms help to prevent it are not well understood.

A key pathomechanism in ALS/FTD cases with FUS aggregates is defective nuclear import. Mutations in *FUS* that cause familial ALS (ALS-FUS) (Kwiatkowski et al., 2009; Vance et al., 2009) often alter or entirely delete the C-terminal nuclear localization signal (NLS) and thus impair nuclear import of FUS (Dormann et al., 2010). The NLS consists of a C-terminal proline tyrosine (PY)-NLS (Lee et al., 2006) and the preceding arginine/glycine-rich RGG3 domain (Dormann et al., 2012). Both domains interact with the nuclear import receptor Transportin (TNPO1)/Karyopherin-β2 (Kapβ2) (Lee et al., 2006), which translocates FUS across the nuclear pore complex into the nucleoplasm. Reduced TNPO1 binding and impaired nuclear import of FUS is pathogenic, as *FUS* mutations that lead to severely reduced TNPO1 binding cause early ALS onset and rapid disease progression (Dormann et al., 2010). This phenotype was recently modeled in mice, where FUS-NLS mutations cause motor neuron degeneration (Devoy et al., 2017; Scekic-Zahirovic et al., 2017).

Defective nuclear import also plays a role in FTD cases with FUS pathology (FTD-FUS), which are usually not associated

with *FUS* mutations (Snowden et al., 2011). In these cases, TNPO1 is aggregated and partially detergent-insoluble (Brelstaff et al., 2011; Neumann et al., 2012). Moreover, arginine methylation (arg-methylation), which regulates TNPO1 binding and nuclear import of FUS, is defective in FTD-FUS patients (Dormann et al., 2012; Suárez-Calvet et al., 2016). Arg-methylation is a common post-translational modification (PTM) in nuclear RBPs, often regulating their nuclear localization, as well as protein-protein or protein-RNA interactions (Bedford and Clarke, 2009). Arg-methylation is carried out by protein arginine methyltransferases (PRMTs), which transfer one or two methyl groups from S-adenosyl-methionine (SAM) onto the arginine side chain (Yang and Bedford, 2013). FUS contains three arginine-glycine-glycine (RGG) repeat domains with RGG/RG motifs that are extensively modified with asymmetric dimethyl groups by PRMT1 or PRMT8 (Ong et al., 2004; Scaramuzzino et al., 2013). We have previously shown that arginine dimethylation is lost in FTD-FUS patients. Instead, deposited FUS is un- or monomethylated (Dormann et al., 2012; Suárez-Calvet et al., 2016). However, it is still unclear whether loss of FUS arg-methylation is pathogenic and contributes to FUS dysfunction or aggregation.

We and others have previously proposed that FUS aggregation is initiated in stress granules (SGs), as ALS-associated FUS-NLS mutations cause an accumulation of FUS in SGs, and FUS aggregates in ALS/FTD *post mortem* brains often contain SG marker proteins (Dormann et al., 2010; Li et al., 2013). Thus, SGs or other ribonucleoprotein (RNP) granules may act as condensation sites, where aggregation-prone RBPs start to aggregate once they exceed a critical concentration. Recently, it has been shown that FUS and related RBPs undergo concentration-dependent, reversible liquid-liquid phase separation (LLPS) *in vitro*, i.e., they form liquid-like protein droplets that have similar dynamic properties as cellular RNP compartments. Over time, liquid FUS and hnRNP-A1 droplets undergo an irreversible "liquid-to-solid phase transition" and form solid, fibrous aggregates *in vitro* (Molliex et al., 2015; Patel et al., 2015). LLPS and liquid-to-solid phase transition of FUS is concentration dependent (Patel et al., 2015); hence, the high local concentration of FUS in SGs may promote LLPS and solidification of FUS.

In the case of FUS, LLPS and aggregation are reported to be largely driven by the N-terminal SYGQ-rich domain (Burke et al., 2015; Kato et al., 2012; Murakami et al., 2015; Patel et al., 2015; Sun et al., 2011), which has a similar amino acid composition as yeast prion domains (King et al., 2012). Here, we show that the C-terminal RGG3-PY domain and arginines in RGG motifs of FUS are also crucial for phase separation of FUS. We demonstrate that TNPO1, which directly interacts with arginines in the RGG3-PY domain, acts as a FUS chaperone and suppresses phase separation and SG association of FUS. Furthermore, we establish that arg-methylation of FUS reduces LLPS and SG association of FUS, suggesting that loss of arg-methylation, as seen in FTD-FUS patients, is pathogenic by directly promoting FUS aggregation. Finally, we show that the ALS-associated FUS-P525L mutation renders the protein less sensitive to the chaperone activity of TNPO1 and thus not only impairs nuclear import, but also enhances phase separation and SG accumulation of mutant FUS. Our findings reveal two novel regulatory mechanisms of liquid phase homeostasis that are disrupted in FUS-associated ALS and FTD. This supports the view that phase separation and SG accumulation of FUS are crucially involved in ALS/FTD pathogenesis.

RESULTS

Transportin Suppresses Phase Transitions of FUS *In Vitro*

As several Importin β (Impβ)-type nuclear import receptors were shown to act as cytoplasmic chaperones of positively charged ribosomal proteins and histones (Jäkel et al., 2002), we hypothesized that TNPO1 may exert a similar function toward other positively charged import cargoes, including FUS. To test whether TNPO1 affects phase transitions of FUS, we purified MBP-FUS-EGFP-His_6 and MBP-FUS-His_6 (see scheme in Figure S1A) from *E. coli*. At physiological FUS concentrations, both proteins were soluble and dispersed, whereas proteolytic removal of the MBP-tag with TEV protease caused them to phase separate and form numerous liquid-like droplets (Figures 1A and S1B). To verify that droplet formation was not induced by TEV protease independently of proteolytic cleavage, we used MBP-FUS containing a *PreScission* cleavage site, which formed droplets upon addition of PreScission protease, but not upon addition of TEV protease (Figure S1B).

To assess how TNPO1 affects LLPS of FUS, we added equimolar amounts of purified TNPO1 or buffer only to MBP-FUS-EGFP and monitored TEV cleavage-induced FUS droplet formation. Strikingly, droplet formation was significantly suppressed by TNPO1 (Figures 1A; see Figure 1B for quantification). Moreover, when TNPO1 was added to preformed FUS droplets, they immediately dissolved (Figure S1C), indicating that TNPO1 is able to reverse LLPS of FUS. Two other direct FUS interactors (Figure S1D), PRMT1 (Scaramuzzino et al., 2013) and an anti-FUS-RGG3-specific antibody (Suárez-Calvet et al., 2016), were unable to suppress FUS droplet formation to the same degree as TNPO1 (Figures 1A and 1B). Likewise, the nuclear import receptor Importin 5 (Imp5), which is not the cognate importin of FUS and does not bind to FUS *in vitro* (Figure S1D), also did not suppress LLPS of FUS (Figures 1A and 1B).

Next, we monitored phase separation of non-EGFP-tagged FUS in a turbidity assay, where the optical density of the protein solution is used as a measure of phase separation. The solution became turbid upon TEV cleavage of MBP-FUS in the presence of buffer, PRMT1, anti-FUS-RGG3 antibody, or Imp5, whereas turbidity remained low in the presence of TNPO1 (Figure 1C). Second, we used a sedimentation assay, where samples are centrifuged, and partitioning of FUS into the pellet fraction is used as a measure of phase separation. Upon TEV cleavage, FUS quantitatively entered the pellet fraction but remained mainly in the supernatant when TNPO1 was present (Figure 1D; see Figure 1E for quantification). In contrast, PRMT1, the FUS-RGG3-specific antibody, or Imp5 were unable to prevent partitioning of FUS into the pellet fraction.

Finally, we performed *in vitro* "aging" experiments, in which liquid FUS droplets are incubated for a few hours with mild

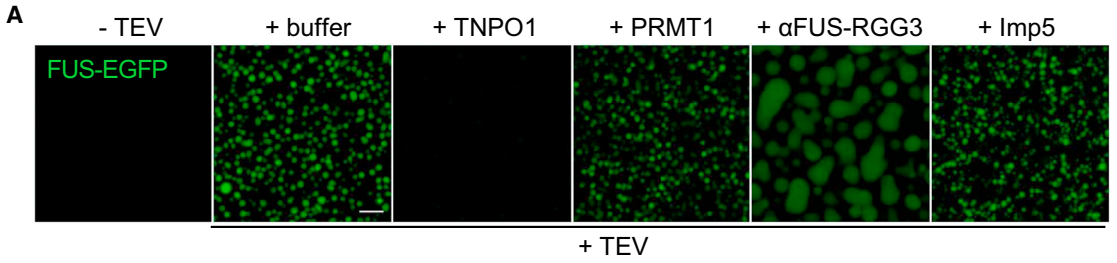

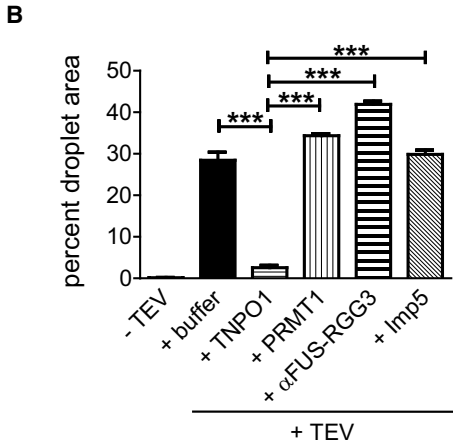

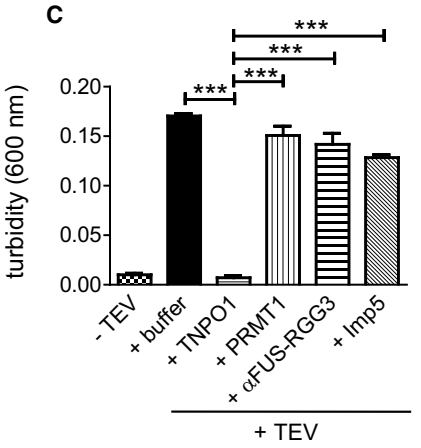

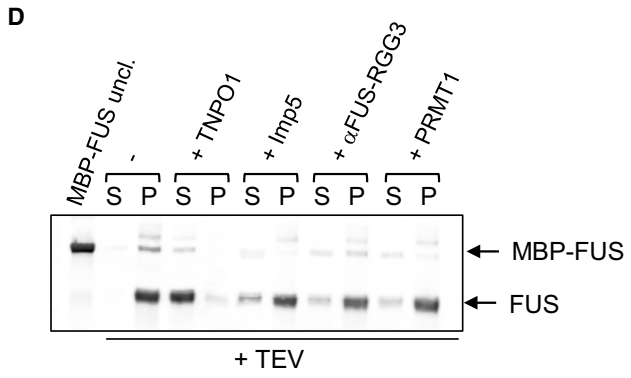

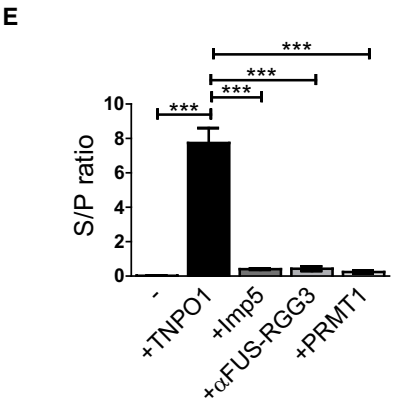

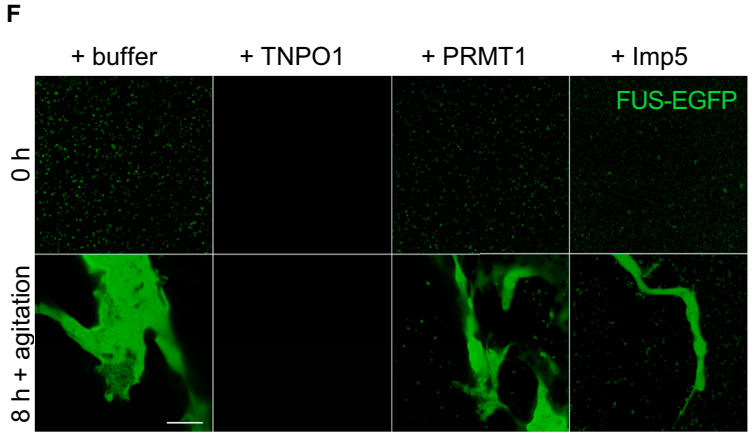

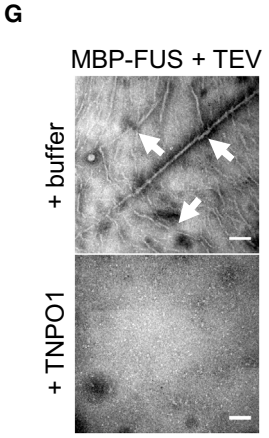

(legend on next page)

agitation and thus are converted into large amorphous aggregates over time (Patel et al., 2015). Addition of TNPO1, but not PRMT1 or Imp5, prevented formation of amorphous FUS-EGFP structures that normally formed during *in vitro* aging (Figure 1F). Similarly, after a 90-min *in vitro* incubation of TEV-cleaved MBP-FUS, transmission electron microscopy (TEM) revealed the presence of rod-like FUS fibrils, which was prevented in the presence of TNPO1 (Figure 1G).

Together, these results demonstrate that TNPO1 appears to have a dual function and not only mediates nuclear import of FUS, but also acts as a chaperone and suppresses LLPS and consequent solidification of FUS *in vitro*.

Transportin Reduces SG Association of FUS, Independent of Its Nuclear Import Activity

TNPO1 is expected to exert its chaperone function toward FUS mainly in the cytoplasm, where RanGTP levels are low and TNPO1 binds tightly to PY-NLS-containing cargoes (Lee et al., 2006). To test whether TNPO1 indeed acts a chaperone of FUS in cells, we expressed a cytosolically anchored version of FUS (GCR_2-tagRFP_2-FUS) in HeLa cells. This fusion protein is retained in the cytoplasm by a hormone-responsive domain of the glucocorticoid receptor (GCR) (Love et al., 1998). We interfered with FUS-TNPO1 binding by co-expressing a peptide inhibitor of TNPO1, EGFP-M9M, which binds TNPO1 with unnaturally high affinity and competes with natural TNPO1 cargoes (Cansizoglu et al., 2007). As a control, we expressed an Importin α (Impα)-specific high-affinity peptide inhibitor (EGFP-bimax) that interferes with Impα-cargo binding and Impα/β-dependent nuclear import (Kosugi et al., 2008). In cells expressing bimax, cytosolically anchored FUS remained diffusely distributed, whereas in cells expressing M9M, FUS was localized in TIA1-positive SGs in a significant number of cells (Figures 2A and 2B). Note that M9M-expressing cells had similar or lower expression levels of GCR_2-tagRFP_2-FUS than bimax-expressing cells (data not shown). This suggests that impaired FUS-TNPO1 binding favors partitioning of cytosolic FUS into SGs.

To directly test the hypothesis that TNPO1 suppresses SG association of FUS, we utilized a modified version of the semi-permeabilized cell assay that is routinely used to study nuclear transport of proteins under defined conditions (Adam et al., 1990). We elicited SGs by treating HeLa cells with the proteasome inhibitor MG132 and then selectively permeabilized the plasma membrane using digitonin and washed out soluble factors, including importins (see scheme in Figure 2C). To focus only on the cytosolic function of TNPO1, we prevented nuclear import by blocking nuclear pores with wheat germ agglutinin (WGA) (Yoneda et al., 1987). Upon addition of MBP-FUS-EGFP to semi-permeabilized cells, the protein specifically associated with G3BP1-positive SGs (Figure 2D). Consistent with our hypothesis, SG association was significantly reduced when TNPO1 was added together with FUS (Figures 2D and 2E).

In summary, our data show that TNPO1 reduces partitioning of FUS into SGs independent of its nuclear import activity. This demonstrates that TNPO1 not only suppresses phase transitions of FUS *in vitro*, but also acts as a FUS chaperone in the cytoplasm, thus reducing the risk of aberrant FUS phase transitions in SGs.

C-Terminal RGG/RG Motifs Are Crucial for Phase Separation of FUS

FUS contains extended disordered LC domains, including the N-terminal SYGQ-rich domain and C-terminal RGG domains enriched in RGG/RG motifs (Figure 3A). Even though LLPS and aggregation of FUS is thought to be largely driven by the N-terminal SYGQ-rich domain (Kato et al., 2012; Patel et al., 2015; Sun et al., 2011), there is evidence that C-terminal regions, in particular RGG/RG-rich domains, contribute to phase separation and aggregation of FUS (Boeynaems et al., 2017; Schwartz et al., 2013). As TNPO1 binds to the C-terminal RGG3-PY domain, we speculated that this domain critically contributes to phase separation of FUS and that TNPO1 may achieve chaperoning of FUS by interacting with LLPS-promoting RGG/RG motifs.

To test this hypothesis, we purified the C-terminal RGG3-PY domain (see Figure S2A for sequence) from *E. coli* and tested its ability to phase separate. In the presence of substoichiometric amounts of RNA, RGG3-PY formed liquid droplets in a concentration- and temperature-dependent manner (Figures 3B and S2B), similar to the N-terminal SYGQ-rich domain (Burke et al., 2015). Formation of RGG3-PY droplets was enhanced at lower salt concentrations (Figure S2C), suggesting that electrostatic interactions involving RGG/RG motifs drive LLPS of this domain. To investigate the importance of arginines in LLPS of RGG3-PY, we expressed and purified a mutant version, termed KGG3-PY, in which all arginines in RGG motifs were replaced by lysine (K) (see Figure S2A). Strikingly, KGG3-PY remained completely dispersed and did not form any visible droplets under conditions

Figure 1. TNPO1 Suppresses Phase Transitions of FUS *In Vitro*

(A) Droplet formation of 7 μM MBP-FUS-EGFP upon TEV cleavage is suppressed by TNPO1, but not by PRMT1, Imp5, or a monoclonal antibody specific for FUS-RGG3. Bar, 10 μm.

(B) Quantification of FUS-EGFP droplets. Values represent means ± SEM (n = 3). ***p < 0.001 by one-way ANOVA with Dunnett's multiple comparison test.

(C) Turbidity assay to quantify phase separation of 7 μM MBP-FUS upon TEV cleavage ± TNPO1, PRMT1, Imp5, or anti-FUS-RGG3 antibody, respectively. Values represent means ± SEM (n = 3). ***p < 0.001 by one-way ANOVA with Dunnett's multiple comparison test.

(D) Sedimentation assay to quantify phase separation of MBP-FUS after TEV cleavage ± TNPO1 or control proteins (Imp5, anti-FUS-RGG3 antibody, or PRMT1).

(E) Quantification of FUS levels in supernatant (S) and pellet (P) fractions as S/P ratio. Values represent mean ± SEM (n = 3). ***p < 0.001 by one-way ANOVA with Dunnett's multiple comparison test.

(F) TNPO1 prevents LLPS and consequent liquid-to-solid phase transition of FUS-EGFP droplets (7 μM) in an *in vitro* aging assay. Bar, 50 μm.

(G) 7 μM MBP-FUS was incubated for 90 min with TEV protease ± TNPO1 and processed for TEM. Arrows indicate fibrillary FUS assemblies formed upon TEV cleavage. Bar, 200 nm.

See also Figure S1.

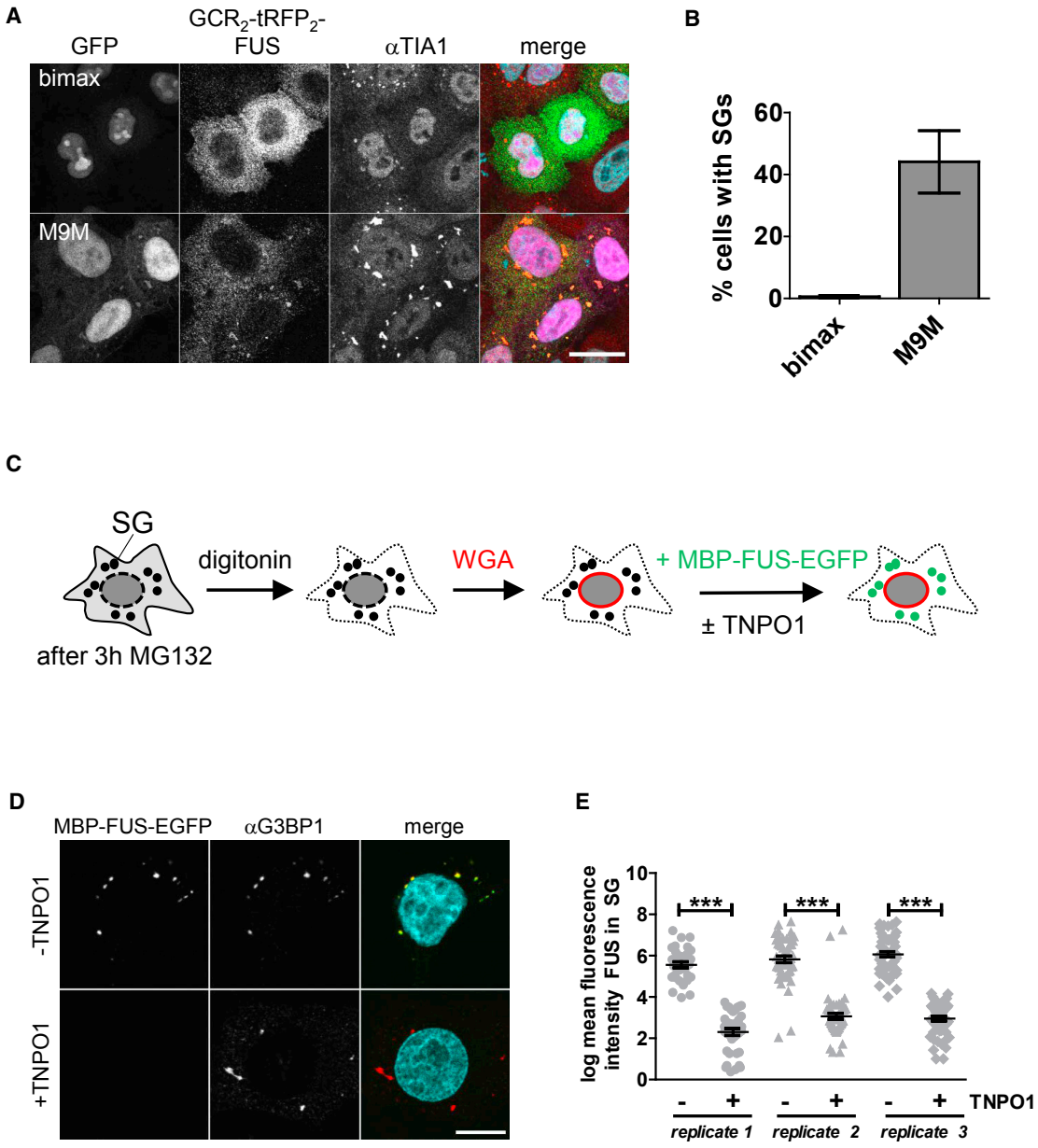

Figure 2. TNPO1 Acts as a FUS Chaperone in Cells and Suppresses SG Association of FUS

(A) Overexpression of the TNPO1-specific inhibitor EGFP-M9M, but not the Impα/β-specific inhibitor EGFP-bimax, results in SG association of cytosolically anchored FUS (GCR_2-tagRFP$_2$-FUS, displayed in green; EGFP displayed in magenta). SGs were identified by TIA1 immunostaining (in red). Nuclei were counterstained with DAPI (turquoise). Bar, 20 μm.

(B) Quantification of cells with GCR_2-tagRFP$_2$-FUS in SGs upon co-expression of either EGFP-bimax or -M9M. Values represent mean ± SEM (n = 3, >100 cells each).

(C) Schematic diagram of the modified semi-permeabilized cell assay. After SG induction with MG132, the plasma membrane is selectively permeabilized by digitonin, and soluble proteins are washed out. To prevent nuclear import, nuclear pores are blocked by WGA before addition of MBP-FUS-EGFP ± TNPO1. After extensive washing, SGs are visualized by G3BP1 immunostaining, and recruitment of FUS into SGs is monitored by EGFP fluorescence.

(D) TNPO1 prevents recruitment of MBP-FUS-EGFP into SGs in semi-permeabilized cells. Nuclei were counterstained with DAPI (turquoise). Bar, 10 μm.

(E) Quantification of the log-transformed mean fluorescence intensity of MBP-FUS-EGFP in SGs for three replicates ± SEM (≥10 cells, ≥32 SGs each). ***$p < 0.001$ by Mann-Whitney test.

that induced large RGG3-PY droplets (Figure 3B). This demonstrates that arginines in RGG motifs are crucial for LLPS of the RGG3-PY domain.

To test whether the C-terminal RGG3-PY domain and arginine residues in RGG/RG motifs are important for phase separation of full-length FUS, we purified two mutant versions of MBP-FUS

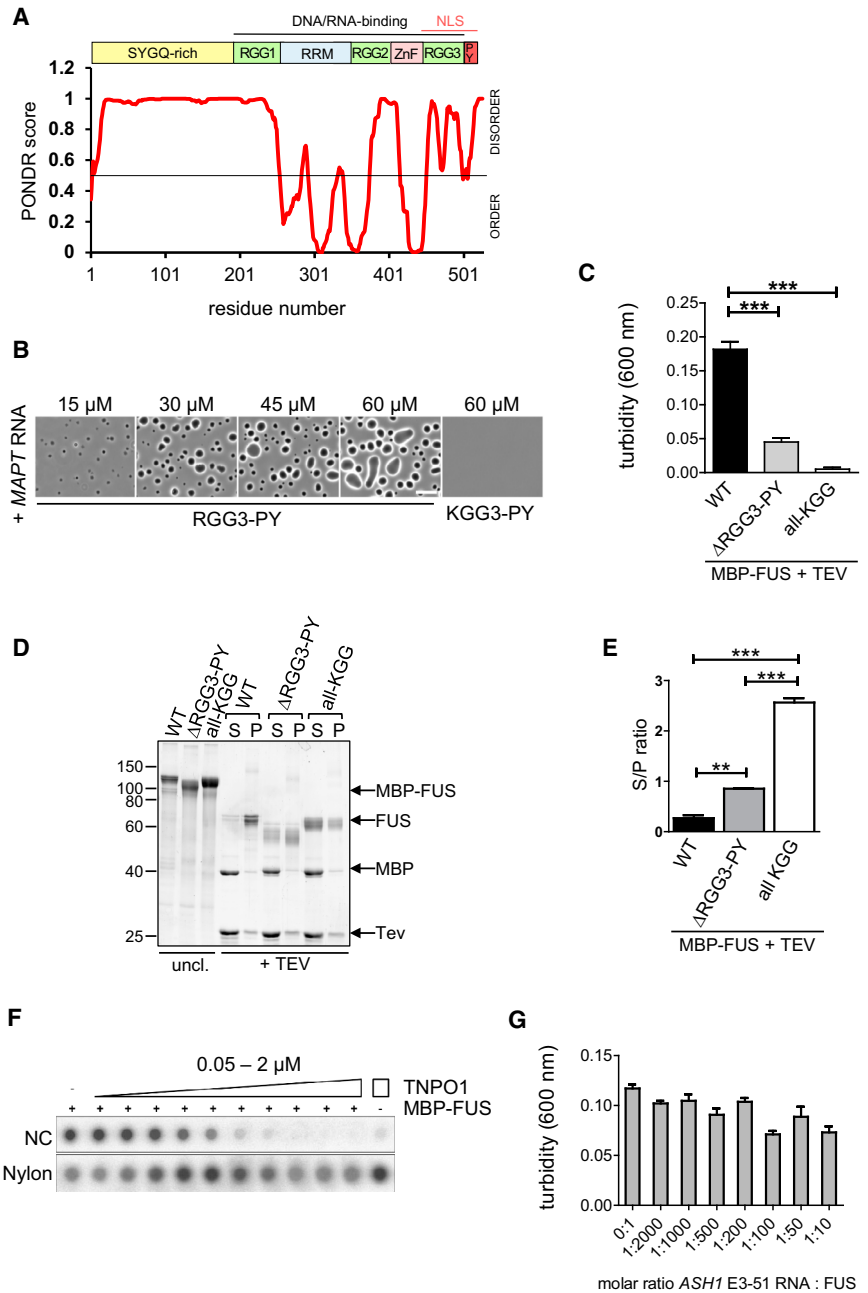

Figure 3. C-Terminal RGG/RG Motifs Crucially Contribute to LLPS of FUS

(A) Schematic diagram of FUS domains and order/disorder prediction by the PONDR algorithm.

(B) Upon addition of substoichiometric amounts of *MAPT* RNA, RGG3-PY forms liquid-like droplets at indicated protein concentrations. A KGG3-PY mutant does not form droplets at 60 μM. Bar, 10 μm.

(C) Turbidity measurement to quantify phase separation of MBP-FUS-ΔRGG3-PY and MBP-FUS-all-KGG in comparison to MBP-FUS-WT (7 μM) upon TEV cleavage. Values represent means ± SEM (n = 3). ***p < 0.001 by one-way ANOVA with Dunnett's multiple comparison test.

(D) Sedimentation assay to quantify phase separation of MBP-FUS-WT in comparison to MBP-FUS-ΔRGG3-PY and MBP-FUS-all-KGG by TEV cleavage in the presence of 150 mM NaCl.

(E) Quantification of the FUS levels in supernatant (S) and pellet (P) fractions as S/P ratio. Values represent mean ± SEM (n = 3). **p < 0.01 and ***p < 0.001 by one-way ANOVA with Bonferroni multiple comparisons test.

(F) Representative images of RNA-protein binding (nitrocellulose: NC) and of free RNA (nylon membrane) in filter binding assays with MBP-FUS, TNPO1, and radioactively labeled *ASH1* E3-51 RNA. Addition of 1 μM MBP-FUS showed significant RNA binding, while increasing amounts of TNPO1 resulted in a separation of proteins (NC) from RNA (nylon).

(G) *ASH1* E3-51 RNA has no influence on phase separation of 5 μM MBP-FUS after TEV cleavage in a turbidity assay. Values represent means ± SEM (n = 3).

See also Figure S2.

where we either deleted the C-terminal RGG3-PY domain (ΔRGG3-PY) or mutated all arginines in RGG/RG motifs to lysine (all-KGG) (see Figure S2D for western blot characterization). In a turbidity assay, FUS wild-type (FUS-WT) showed a strong turbidity increase, whereas FUS-ΔRGG3-PY yielded lower turbidity values, and the all-KGG mutant failed to become turbid at all (Figure 3C). Sedimentation analysis confirmed that ΔRGG3-PY shows reduced partitioning into the pellet fraction compared to FUS-WT, and the all-KGG mutant remained mostly soluble (Figures 3D and 3E). Thus, phase separation of FUS not only requires the N-terminal SYGQ-rich domain, but also arginine residues in C-terminal RGG/RG motifs.

Molecular Mechanisms Contributing to Chaperoning of FUS by TNPO1

Based on this finding, we considered two not mutually exclusive hypotheses as to how TNPO1 may suppress LLPS of FUS. First, as RGG/RG motifs were shown to be crucial for RNA binding of FUS (Ozdilek et al., 2017), we considered the possibility that TNPO1 may compete with RNA binding to RGG/RG motifs and hence suppress RNA-driven LLPS of FUS. Second, TNPO1 may directly interact with arginines and thus interfere with arginine-driven LLPS of FUS.

To address the first hypothesis, we performed nuclear magnetic resonance (NMR) spectroscopy and examined the effect of TNPO1 on RNA-driven phase separation of the RGG3-PY domain. Addition of increasing amounts of unlabeled RNA to ^{15}N-labeled RGG3-PY caused the sample to become turbid (data not shown) and led to progressive disappearance of ^{1}H-^{15}N cross peaks (Figure S2E) and decreased signal intensity in the corresponding 1D NMR spectra (Figure S2F). This is in agreement with the formation of high-molecular-weight RGG3-PY/RNA droplets, leading to broadening of NMR signals due to

the decreased rotational tumbling time of the RGG3 region within droplets. RNA was quantitatively bound by RGG3-PY droplets, as NMR signals of unlabeled RNA were absent in the 1D NMR spectra (Figure S2F). Addition of TNPO1 to the RGG3-PY/RNA droplet sample led to reappearance of the RNA ^{1}H NMR signals (Figure S2F) and a loss of turbidity, indicating that TNPO1 binding displaces the RNA from RGG3-PY and results in droplet dissolution. Concordantly, radioactive filter binding experiments demonstrated that RNA is displaced from full-length FUS upon addition of TNPO1 (Figures 3F and S2G). However, in the turbidity assay, we did not detect an altered phase separation behavior of full-length FUS upon titrating in *ASH1* E3-51 RNA (Figure 3G); similar results were obtained for *MAPT* RNA and total RNA (data not shown). This suggests that phase separation of full-length FUS is not strongly affected by RNA under our experimental conditions. Hence, the displacement of RNA from FUS might not be the major mechanism by which TNPO1 suppresses phase separation of FUS.

In support of the second hypothesis, namely that TNPO1 interferes with phase separation of FUS by interacting with arginines in the C-terminal RGG3-PY domain, we have previously shown that TNPO1 directly binds to a synthetic FUS-RGG3 peptide (Dormann et al., 2012) and to several arginine residues in the FUS-RGG3 region (R472, R473, R476) (Göbl et al., 2016). This interaction appears to be mainly charge-driven, as we observed a strong decrease in binding of TNPO1 to RGG3-PY at higher salt concentration (Figure S4A and Table S1). Together, our previously published data and our isothermal titration calorimetry (ITC) results show that electrostatic interactions and arginine residues play a key role in binding of RGG3-PY to TNPO1. As arginine residues and the C-terminal RGG3-PY domain of FUS appear to be crucial for phase separation of FUS (Figures 3B–3E), we propose that direct binding of TNPO1 to arginines in the RGG3-PY domain interferes with arginine-driven phase separation of FUS and thus could be an important component of the chaperoning mechanism.

Arginine Methylation Reduces LLPS and SG Association of FUS

As arginines in RGG/RG motifs have an important contribution to LLPS of FUS (Figures 3B–3E), we asked how arg-methylation alters phase separation of FUS. This question is of great interest, as arg-dimethylation of the FUS-RGG3 domain is lost in FTD-FUS patients (Dormann et al., 2012; Suárez-Calvet et al., 2016), but it is unclear whether and how loss of FUS methylation is pathogenic.

To address this question, we *in vitro* methylated purified MBP-FUS-EGFP, MBP-FUS, or RGG3-PY by adding the purified arginine methyltransferase PRMT1 and SAM as a methyl donor (Figure S3A). FUS proteins were purified from bacteria and therefore were originally unmethylated. After incubation with PRMT1 and SAM, all three proteins were efficiently converted from an un- to a dimethylated form but remained unmethylated upon incubation with PRMT1 only (Figure S3B; similar results for MBP-FUS and RGG3-PY, data not shown). First, we examined the propensity of unmethylated and methylated MBP-FUS-EGFP to undergo LLPS and found that unmethylated FUS formed liquid droplets at lower concentrations than dimethylated FUS (Figure 4A). This difference was not caused by the methyl donor SAM, as addition of SAM alone did not alter droplet formation (data not shown). Compared to dimethylated FUS, unmethylated FUS also showed reduced internal mobility within the dense droplet phase as measured by fluorescence recovery after photobleaching (FRAP) following a "half bleach" of FUS-EGFP droplets (Figures 4B and 4C). Moreover, in a turbidity assay, unmethylated FUS reached higher turbidity values than methylated FUS (Figure 4D). Sedimentation analysis confirmed that unmethylated FUS had a higher propensity to partition into the pellet fraction compared to methylated FUS (Figures S3C and S3D). Enhanced phase separation was also observed for the unmethylated RGG3-PY domain, which reached higher turbidity values than methylated RGG3-PY upon addition of RNA (Figure S3E). This difference was not due to altered RNA binding, as filter binding experiments demonstrated equal affinity of unmethylated and methylated RGG3-PY for RNA (Figures S3F and S3G and Table S2).

To transfer these findings into cells, we investigated whether arg-methylation affects SG association of FUS in the semi-permeabilized cell assay. Indeed, unmethylated FUS showed a higher association with G3BP1-positive SGs compared to the methylated protein (Figures 4E and 4F). This suggests that unmethylated FUS associates with SGs more stably than methylated FUS. In conclusion, loss of FUS arg-methylation, as seen in FTD-FUS patients, promotes LLPS and SG partitioning of FUS and thus may contribute to FUS aggregation in FTD-FUS patients.

The ALS-Associated FUS-P525L Mutation Renders FUS Less Sensitive to the Chaperone Activity of TNPO1

Most ALS patients with FUS pathology carry a mutation in the PY-NLS that causes reduced binding to TNPO1 and impairs nuclear import of FUS (Dormann et al., 2010; Zhang and Chook, 2012). Given our finding that TNPO1 suppresses LLPS and SG association of FUS, we hypothesized that FUS PY-NLS mutations may also impair chaperoning of FUS by TNPO1 and thus promote aberrant phase transitions and SG partitioning of mutant FUS.

To test this hypothesis, we purified MBP-FUS-EGFP and the RGG3-PY domain with an intact or mutant (P525L) PY-NLS. The P525L mutation severely weakens TNPO1 binding (Zhang and Chook, 2012) and causes early-onset ALS and rapid disease progression (Chiò et al., 2009). As the FUS-RGG3 domain is normally arg-methylated in ALS-FUS patients, and this furthermore weakens TNPO1 binding (Dormann et al., 2012) (Figures S4A and S4B and Table S1), we *in vitro* methylated WT and mutant proteins (Figure S4C) and then examined their ability to phase separate in the presence and absence of TNPO1. Without TNPO1, mutant and WT proteins formed liquid droplets to a similar extent (Figures 5A and 5B); hence, the P525L mutation does not alter LLPS of FUS under these conditions. In line with our hypothesis, the WT protein was efficiently chaperoned by TNPO1, whereas the mutant protein still formed liquid droplets in the presence of TNPO1, even after prolonged incubation (8 hr) (Figures 5A and 5B).

To test whether the P525L mutation also causes reduced chaperoning by TNPO1 in cells, we examined the ability of

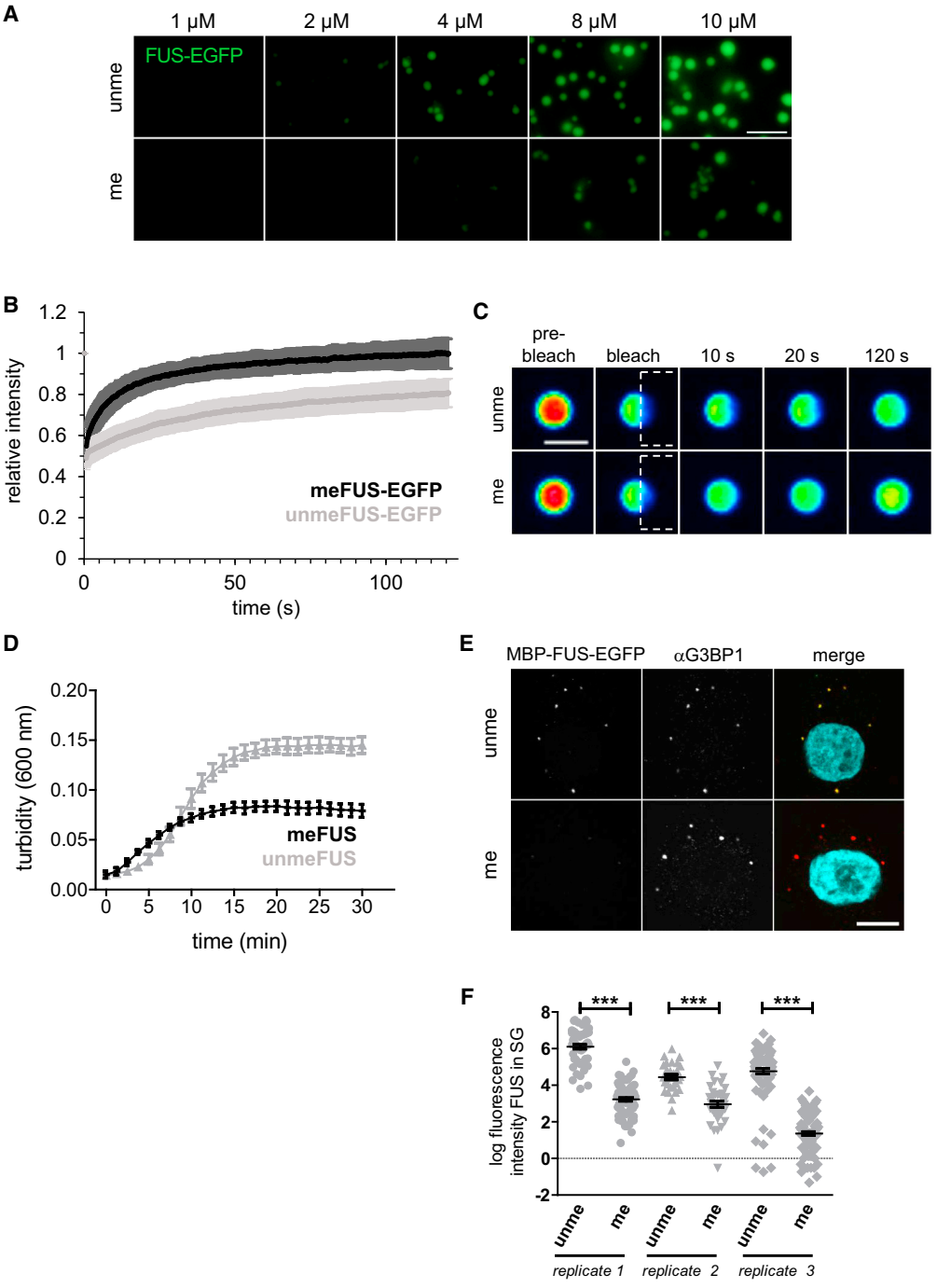

Figure 4. Arginine Methylation of FUS Reduces LLPS and SG Association of FUS

(A) Droplet formation for unmethylated (unme) or methylated (me) FUS-EGFP at different protein concentrations following TEV cleavage of MBP-FUS-EGFP. Bar, 5 μm.

(B) FRAP curves after half-bleach of 9 μM unmethylated (unme) or methylated (me) FUS-EGFP droplets (75 mM NaCl supplemented with 150 mg/mL Ficoll 400). Values represent means ± SD (n = 33). Representative pictures of indicated time points are shown in (C). Boxes indicate bleached area. Bar, 2 μm.

(D) Turbidity measurement over time to determine phase separation of 7 μM unmethylated (unme) or methylated (me) MBP-FUS in the presence of 75 mM NaCl upon TEV cleavage. Values represent means ± SEM (n = 3).

(E) Enhanced SG recruitment of unmethylated (unme) MBP-FUS-EGFP compared to methylated (me) MBP-FUS-EGFP in semi-permeabilized cells. Bar, 10 μm.

(F) Quantification of the log-transformed mean fluorescence intensity of MBP-FUS-EGFP in SGs for three replicates ± SEM (≥10 cells, ≥28 SGs each). ***p < 0.001 by Mann-Whitney test.

See also Figure S3 and Table S2.

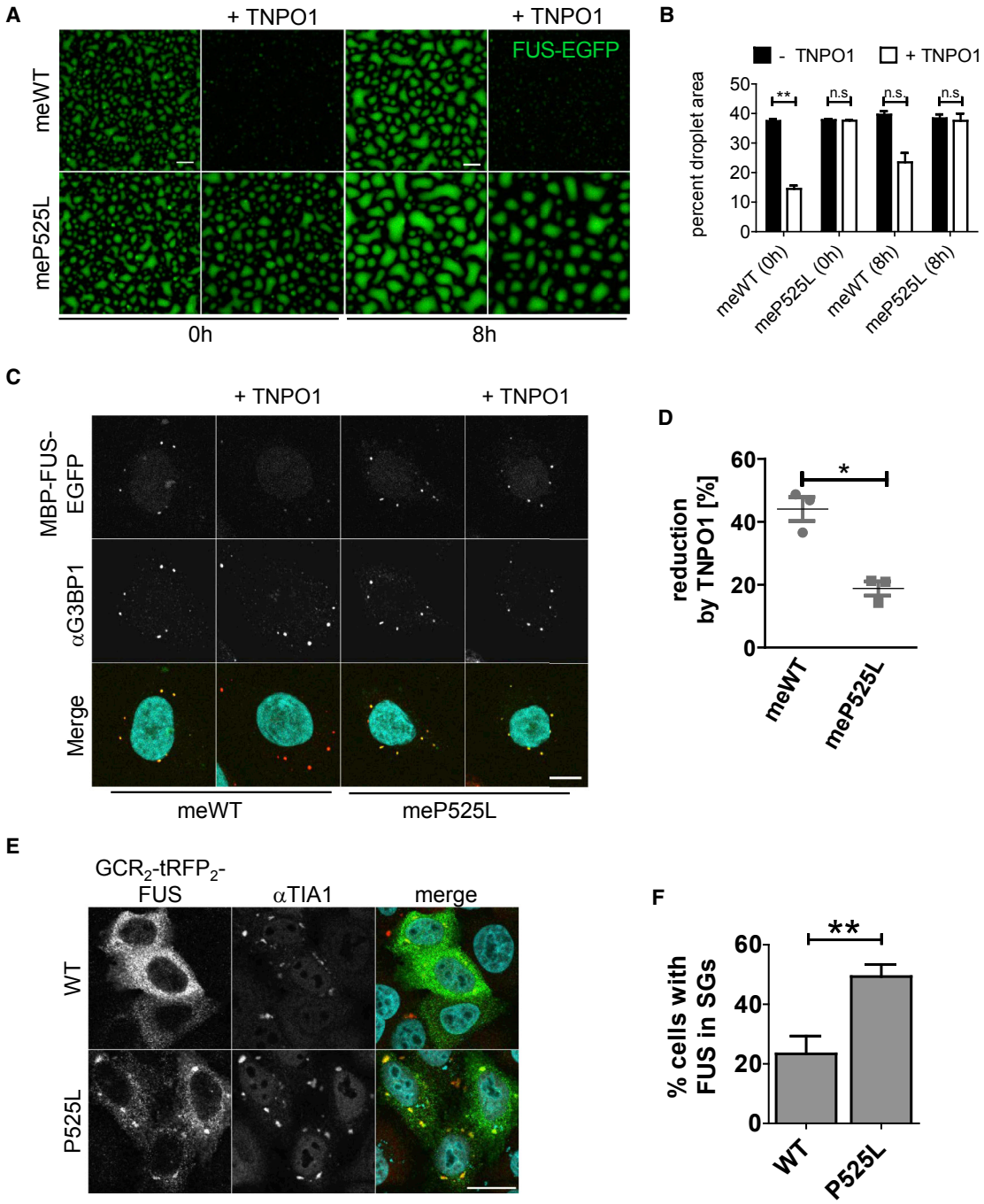

Figure 5. The ALS-Associated FUS-P525L Mutation Impairs the Chaperone Activity of TNPO1

(A) Droplet formation after TEV cleavage of methylated 11 μM MBP-FUS-EGFP WT versus P525L ± TNPO1 after 0 and 8 hr. Bar, 15 μm.

(B) Percentage of image area covered by FUS-EGFP droplets. Values represent means ± SEM (n = 3). **$p < 0.01$ by paired t test.

(C) SG association of WT versus P525L MBP-FUS-EGFP ± TNPO1 in the semi-permeabilized cell assay. Nuclei were counterstained with DAPI (turquoise). Bar, 10 μm. Note that image acquisition conditions differed from the experiment shown in Figure 4E to visualize methylated FUS in SGs without TNPO1.

(D) The mean reduction of SG association of FUS (-TNPO1 set to 100%) was calculated from three independent experiments. (≥10 cells, ≥37 SGs each). *$p < 0.05$ by paired t test.

(E) SG recruitment of cytosolically anchored (GCR_2-tagRFP$_2$-tagged) FUS-WT or -P525L in HeLa cells was monitored by co-immunostaining for tagRFP (green) and TIA1 (red). Nuclei were counterstained with DAPI (turquoise). Bar, 20 μm.

(F) The percentage of cells showing SG-localized GCR_2-tagRFP$_2$-FUS. Values represent mean ± SEM (n = 3 with n >100 cells each). **$p<0.01$ by paired t test.

See also Figure S4 and Table S1.

TNPO1 to suppress SG association of WT versus mutant MBP-FUS-EGFP in the semi-permeabilized cell assay. Both WT and mutant proteins showed a similar SG association; however, addition of TNPO1 reduced SG partitioning of the WT protein but was significantly less efficient in chaperoning the P525L mutant protein (Figures 5C and 5D). This was not due to better nuclear import of the WT protein, as nuclear pores were blocked in this assay by WGA.

Finally, we tested whether the P525L mutation favors SG partitioning of FUS in intact and living cells independent of reduced nuclear import. To do so, we used the GCR-based cytosolic anchoring system and expressed GCR_2-tagRFP$_2$-tagged FUS-WT or P525L in HeLa cells. Both fusion proteins are localized in the cytoplasm (Figure 5E) and reached similar expression levels (data not shown). In cells where TIA1-positive SGs were elicited due to transfection stress, the WT protein was predominantly diffusely distributed in the cytoplasm and showed little SG association, whereas the P525L mutant protein frequently co-localized with TIA1-positive SGs (Figures 5E and 5F).

Together, our *in vitro* and cellular data show that ALS-associated *FUS*-NLS mutations that strongly reduce TNPO1 binding not only impair nuclear import of FUS, but also render the protein less sensitive to the chaperoning activity of TNPO1. Hence, such mutations have an unexpected novel pathomechanism and favor aberrant phase transitions and SG partitioning of mutant FUS in the cytoplasm.

DISCUSSION

The Nuclear Import Receptor TNPO1 Acts as a Cytoplasmic Chaperone of FUS

FUS is among the top 5% of proteins in terms of protein abundance (Wiśniewski et al., 2014), hence its cellular concentration (~2–10 μM) is close to the critical concentration where purified FUS undergoes LLPS and liquid-to-solid phase transition *in vitro* (Patel et al., 2015). This suggests that efficient protein quality control (PQC) mechanisms prevent such aberrant phase transitions in cells. Our data demonstrate that TNPO1 fulfills such a PQC function and suppresses aberrant phase transitions of FUS *in vitro* and in the cytoplasm and decreases the potentially detrimental accumulation of FUS in SGs. SGs are thought to be the sites where FUS (and other aggregation-prone RBPs) get highly concentrated and thus undergo concentration-dependent LLPS and aggregation (Alberti and Hyman, 2016). The importance of SGs for RBP aggregation is underscored by the observation that FUS and TDP-43 aggregates in ALS and FTD patients contain various SG marker proteins (Bentmann et al., 2012; Dormann et al., 2010) and that ALS-causing mutations in FUS or other RBPs promote SG localization or alter SG dynamics (Kim et al., 2013; Mackenzie et al., 2017). Our data show that (1) impaired FUS-TNPO1 binding in cells promotes SG localization of FUS and that (2) TNPO1 directly reduces SG partitioning of FUS. This activity of TNPO1 is independent of its nuclear import function, as nuclear import of FUS was blocked in our cellular assays. Interestingly, TNPO1 and other importins are found in SGs and P bodies (Chang and Tarn, 2009; Fujimura et al., 2010; Weinmann et al., 2009). Our data suggest that chaperoning of aggregation-prone RBPs may be one important function of importins in cytoplasmic RNP granules.

Importins may have a general chaperone function toward aggregation-prone basic proteins, as several other Impβ-type nuclear import receptors were shown to prevent aggregation of basic ribosomal proteins and histones (Jäkel et al., 2002) and phenylalanine-glycine (FG)-rich nucleoporins (Milles et al., 2013). As importins are similarly abundant as heat shock proteins, they appear suited to shield basic stretches on abundant import cargoes, including ALS/FTD-associated RBPs. Indeed, Impα/β prevents and reverses TDP-43 fibrillization, and TNPO1 also inhibits and reverses fibrillization of the PY-NLS-containing cargoes EWS, TAF15, hnRNP-A1, and hnRNP-A2 (Guo et al., 2018).

Arginines in RGG/RG Motifs Are Crucial for Phase Separation of FUS

So far, LLPS and aggregation of FUS were thought to be primarily driven by the N-terminal SYGQ-rich domain (Burke et al., 2015; Kato et al., 2012; Murakami et al., 2015; Patel et al., 2015; Sun et al., 2011). Our data now show that the C-terminal RGG3-PY domain and, in particular, arginines in RGG/RG motifs also play a crucial role in phase separation of FUS. Our findings are consistent with the previous reports that the RGG2-ZnF-RGG3 domain of FUS forms fibrous assemblies *in vitro* (Schwartz et al., 2013) and that a synthetic FUS-RGG3 peptide forms droplets in the presence of a molecular crowder or polyU$_{30}$ (Boeynaems et al., 2017). RGG/RG-rich sequences were also shown to drive phase separation of the *C. elegans* P granule proteins LAF-1 and PGL-3 and the human RNA helicases Ddx4, DDX3X, and EIF4H (Elbaum-Garfinkle et al., 2015; Nott et al., 2015, 2016; Saha et al., 2016). Moreover, arginine-rich dipeptide repeat (DPR) proteins derived from expanded *C9orf72* hexanucleotide repeats phase separate *in vitro* (Boeynaems et al., 2017). In the Ddx4 disordered domain, repeatedly spaced RG/GR and FG/GF dipeptides, suggested to engage in arginine-aromatic (cation-π) interactions, were shown to drive LLPS and droplet formation (Nott et al., 2015). The RGG3-PY domain contains a similar sequence pattern (Figure S2A), with multiple RGG, RG/GR motifs, as well as (F/Y)G or G/(F/Y) dipeptides. As tyrosine (Y) residues in the N-terminal SYGQ-rich domain of FUS were shown to drive hydrogel formation (Kato et al., 2012) and to promote phase separation of a poly-SH3 domain (Lin et al., 2017), it can be speculated that both N-terminal tyrosines and C-terminal arginines crucially contribute to phase separation of FUS and possibly promote LLPS by engaging in tyrosine-arginine (cation-π) interactions.

Multiple Mechanisms May Contribute to the Chaperone Activity of TNPO1

So far, TNPO1 was shown to bind to the FUS-PY-NLS (Zhang and Chook, 2012) and the neighboring RGG3 domain as additional binding epitope (Dormann et al., 2012, Göbl et al., 2016). As arginines in RGG/RG motifs are crucial for efficient phase separation of FUS, we propose that direct TNPO1-arginine interactions contribute to chaperoning of FUS by TNPO1. By

directly interacting with arginines, TNPO1 may suppress weak intermolecular interactions of arginines with other residues (e.g., cation-π interactions) that drive LLPS of FUS, thus suppressing arginine-driven phase transitions.

Beyond this arginine shielding mechanism, weak interactions of TNPO1 with other FUS domains (e.g., the N-terminal SYGQ-rich domain or folded RNA-binding domains [RRM and zinc-finger domain]) (Yoshizawa et al., 2018) may also contribute to the chaperoning activity of TNPO1. It can be speculated that TNPO1 not only has the ability to break weak transient intermolecular interactions between FG-rich nucleoporins as it traverses the nuclear pore, but can also engage in multiple low-affinity interactions with different sites of NLS-bound cargo proteins to keep them soluble in the cytoplasm and during transport. TNPO1-binding to different RNA-binding domains could underlie the RNA displacement that we observed upon addition of TNPO1 to FUS. As RNA has been reported to promote LLPS and aggregation of FUS (Burke et al., 2015; Schwartz et al., 2013), it seems possible that a displacement of RNA by TNPO1 may additionally contribute to the chaperoning mechanism. As we did not find a promoting effect of different types of RNA on phase separation of full-length FUS in our turbidity assay, the exact role of RNA in LLPS and aggregation of FUS needs to be clarified in future studies. Nevertheless, the displacement of RNA from FUS by TNPO1 may have an important function in the cell and ensure that RBPs, such as FUS, are imported in an RNA-free form, thus preventing mRNA reimport into the nucleus. Moreover, it may help to release mRNAs from RBPs for local translation, as reported for the yeast homolog of TNPO1, Kap104p (van den Bogaart et al., 2009).

Arginine Methylation Reduces LLPS and SG Association of FUS

In line with the idea that RGG/RG motifs are crucially involved in phase separation of FUS, we found that arg-methylation of RGG/RG motifs reduces LLPS of FUS and increases droplet dynamics. A similar effect has been reported for the disordered Ddx4 domain and the LC domain of hnRNP-A2 (Nott et al., 2015; Ryan et al., 2018). Although arg-methylation does not alter the positive net charge, it changes hydrogen bonding and local hydrophobicity of arginines (Fuhrmann et al., 2015) and thus may influence cation-π interactions that drive LLPS. It seems likely that LLPS of many more proteins is influenced by arg-methylation, as RGG/RG-rich domains appear to be an important determinant of LLPS, and there are >400 proteins with tri- or di-RGG or tri-RG motifs in the human proteome, many of which are arg-methylated (Thandapani et al., 2013). Prominent examples could be the other two members of the FET (FUS, EWS, TAF15) family, EWS and TAF15, which co-aggregate with FUS in FTD-FUS patients (Neumann et al., 2011) and members of the hnRNP-A family, which form pathological aggregates in rare familial forms of ALS or the related disorder multisystem proteinopathy (Kim et al., 2013; Mori et al., 2013). It will be interesting to see whether arg-methylation is a PTM that generally reduces overly tight interactions between RGG/RG-rich low-complexity domains and thus suppresses aberrant LLPS and aggregation of RGG/RG-rich RBPs.

Distinct Pathomechanisms in FTD-FUS and ALS-FUS Promote Phase Separation and SG Localization of FUS

We have previously shown that aggregated FUS is un- and monomethylated in FTD-FUS patients, whereas it carries arg-dimethyl groups in healthy cells and ALS-FUS patients (Dormann et al., 2012; Suárez-Calvet et al., 2016). We now show that loss of FUS methylation promotes LLPS and SG partitioning of FUS, suggesting that the altered FUS methylation pattern is a pathogenic factor that contributes to the formation of FUS aggregates in patients. What remains to be clarified is why TNPO1 is unable to suppress pathological LLPS and aggregation of hypomethylated FUS in FTD-FUS patients. Efficient chaperoning of hypomethylated FUS by TNPO1 would be expected, as un- and monomethylated FUS show a higher TNPO1 binding affinity than dimethylated FUS (Dormann et al., 2012; Suárez-Calvet et al., 2016) (Figure S4 and Table S1), and LLPS of unmethylated FUS is efficiently suppressed by TNPO1 (this study; Guo et al., 2018; Yoshizawa et al., 2018). One explanation could be that TNPO1 is aggregated and partially detergent-insoluble in *post mortem* brains of FTD-FUS patients (Brelstaff et al., 2011; Neumann et al., 2012) and thus is most likely functionally impaired. Cells with TNPO1 aggregates may have reduced TNPO1 activity, causing impaired nuclear import, enhanced LLPS, and SG partitioning of FUS in the cytoplasm. It can be speculated that loss of FUS methylation may be a compensatory mechanism to increase TNPO1 affinity and thus compensate for reduced TNPO1 activity. How TNPO1 becomes aggregated and how FUS methylation is lost in FTD-FUS patients is unknown. Addressing how TNPO1 levels and FUS methylation are normally regulated and how they can be modulated in cells will be important next steps and may lead to novel therapeutic approaches.

In contrast to FTD-FUS, ALS-FUS patients show a normal methylation pattern (Dormann et al., 2012); however, they often carry a FUS PY-NLS mutation, which reduces TNPO1 binding and impairs nuclear import of FUS (Dormann et al., 2010; Zhang and Chook, 2012). Our study, as well as an accompanying study by Guo et al. (2018), now show that FUS PY-NLS mutations that severely reduce TNPO1 binding, such as P525L and R495X, also reduce the capacity of TNPO1 to act as a chaperone of FUS. Hence, ALS-associated FUS PY-NLS mutations impart a "double hit" and drive (1) cytosolic accumulation due to impaired nuclear import and (2) LLPS and aggregation of FUS in the cytoplasm.

Conclusion

Together, our data reveal two novel mechanisms of liquid-phase homeostasis: (1) arginine methylation and (2) TNPO1 binding. They both suppress phase separation and SG partitioning of FUS and are disrupted in FTD-FUS and ALS-FUS, respectively. These findings support the view that phase separation and the accumulation of FUS in SGs crucially contribute to the pathogenesis of FUS-associated ALS and FTD. Interestingly, a similar pathomechanism has recently been suggested to underlie the most frequent genetic cause of ALS/FTD, a hexanucleotide repeat expansion in the *C9orf72* gene (Edbauer and Haass, 2016), in which arginine-rich DPR proteins (poly-PR, poly-GR) were shown to undergo LLPS, bind numerous LC domain-containing proteins, disturb LLPS of LC domain-containing proteins, and alter formation and dynamics of membrane-less organelles,

such as SGs and nucleoli (Boeynaems et al., 2017; Lee et al., 2016). Thus, disturbed phase transitions appear to be a common theme in ALS/FTD and possibly other RBP-linked disorders.

STAR★METHODS

Detailed methods are provided in the online version of this paper and include the following:

- KEY RESOURCES TABLE
- CONTACT FOR REAGENT AND RESOURCE SHARING
- EXPERMENTAL MODEL AND SUBJECT DETAILS
  - Cell culture and transfection
  - Bacterial Growth
- METHOD DETAILS
  - Generation of cDNA constructs
  - Recombinant protein expression and purification
  - In vitro methylation
  - In vitro transcription
  - In vitro phase separation assays
  - Semi-permeabilized cell assay
  - Filter binding assay
  - Immunocytochemistry
  - Microscopy
  - Nuclear magnetic resonance
  - Isothermal Calorimetry
- QUANTIFICATION AND STATISTICAL ANALYSIS
  - Statistics
  - Image analysis
  - FRAP analysis
  - Densitometry measurements

SUPPLEMENTAL INFORMATION

Supplemental Information includes four figures and three tables and can be found with this article online at https://doi.org/10.1016/j.cell.2018.03.004.

ACKNOWLEDGMENTS

We thank Michael Kiebler for infrastructure (including SD confocal microscope; DFG INST 86/1581-1 FUGG). We thank Frauke van Bebber, Hilary Wunderlich, Jim Shorter, Yuh Min Chook, and Michael Rosen for critical comments on the manuscript. We are grateful to the Biomedical Center core facilities Bioimaging and Bioinformatics, as well as Bastian Popper, Shovamayee Maharana, Claudia Abou-Ajram, Melanie Fritz, and Daniela Rieger for technical assistance. We thank Michael Kiebler, Angelika Noegel, Elisabeth Kremmer, the Helmholtz Center Munich Monoclonal Antibody Core Facility, Ralph Kehlenbach, Elmar Wahle, Arie Geerlof, Ina Poser, Tony Hyman, Dirk Görlich, Matthias Geyer, Simon Alberti, and Jie Wang for generous gifts of reagents. This work was supported by the Deutsche Forschungsgemeinschaft (DFG) within the Emmy Noether grant DO 1804/1-1 and the Munich Cluster for Systems Neurology (Synergy, EXC 1010), as well as the Investment Fund and Junior Research Fund of the LMU Munich (to D.D.). T.M. is supported by the Integrative Metabolism Research Center Graz of the Austrian infrastructure program 2016/2017, BioTechMed-Graz, Omics Center Graz, the Bavarian Ministry of Sciences, Research, and the Arts (Bavarian Molecular Biosystems Research Network), the President's International Fellowship Initiative of CAS (2015VBB045), the National Natural Science Foundation of China (31450110423), the Austrian Science Fund (FWF: P28854, W1226-B18) as well as the DFG (MA5703/1-1). The research of M.-D.R. was supported by the NOMIS Foundation and the research of A.N.-B. and D.N. was supported by the DFG (FOR2333).

AUTHOR CONTRIBUTIONS

Conceptualization, D.D., M.H., S.H.; Methodology, M.H., S.H., B.B., A.N.-B., M. Schifferer, M. Simons, D.N., T.M., D.D.; Investigation, M.H., S.H., B.B., E.S., A.N.-B., M. Schifferer; Resources, M.-D.R., D.N., M. Simons, T.M., D.D.; Writing—Original Draft D.D., M.H., S.H.; Writing—Review and Editing, D.D., M.H., S.H., T.M., B.B., E.S., A.N.-B., D.N., M.-D.R., M. Schifferer, M. Simons; Visualization, M.H., S.H., A.N.-B., B.B., E.S., T.M., D.D.; Supervision, D.D.; Project Administration, D.D.; Funding Acquisition, D.D., T.M.

DECLARATION OF INTERESTS

The authors declare no competing interests.

Received: April 12, 2017
Revised: November 26, 2017
Accepted: February 28, 2018
Published: April 19, 2018

REFERENCES

Adam, S.A., Marr, R.S., and Gerace, L. (1990). Nuclear protein import in permeabilized mammalian cells requires soluble cytoplasmic factors. J. Cell Biol. *111*, 807–816.

Alberti, S., and Hyman, A.A. (2016). Are aberrant phase transitions a driver of cellular aging? BioEssays *38*, 959–968.

Bedford, M.T., and Clarke, S.G. (2009). Protein arginine methylation in mammals: who, what, and why. Mol. Cell *33*, 1–13.

Bentmann, E., Neumann, M., Tahirovic, S., Rodde, R., Dormann, D., and Haass, C. (2012). Requirements for stress granule recruitment of fused in sarcoma (FUS) and TAR DNA-binding protein of 43 kDa (TDP-43). J. Biol. Chem. *287*, 23079–23094.

Boeynaems, S., Bogaert, E., Kovacs, D., Konijnenberg, A., Timmerman, E., Volkov, A., Guharoy, M., De Decker, M., Jaspers, T., Ryan, V.H., et al. (2017). Phase Separation of C9orf72 Dipeptide Repeats Perturbs Stress Granule Dynamics. Mol. Cell *65*, 1044–1055.

Brelstaff, J., Lashley, T., Holton, J.L., Lees, A.J., Rossor, M.N., Bandopadhyay, R., and Revesz, T. (2011). Transportin1: a marker of FTLD-FUS. Acta Neuropathol. *122*, 591–600.

Burke, K.A., Janke, A.M., Rhine, C.L., and Fawzi, N.L. (2015). Residue-by-Residue View of In Vitro FUS Granules that Bind the C-Terminal Domain of RNA Polymerase II. Mol. Cell *60*, 231–241.

Cansizoglu, A.E., Lee, B.J., Zhang, Z.C., Fontoura, B.M., and Chook, Y.M. (2007). Structure-based design of a pathway-specific nuclear import inhibitor. Nat. Struct. Mol. Biol. *14*, 452–454.

Chang, W.L., and Tarn, W.Y. (2009). A role for transportin in deposition of TTP to cytoplasmic RNA granules and mRNA decay. Nucleic Acids Res. *37*, 6600–6612.

Charneau, P., Mirambeau, G., Roux, P., Paulous, S., Buc, H., and Clavel, F. (1994). HIV-1 reverse transcription. A termination step at the center of the genome. J. Mol. Biol. *241*, 651–662.

Chiò, A., Restagno, G., Brunetti, M., Ossola, I., Calvo, A., Mora, G., Sabatelli, M., Monsurrò, M.R., Battistini, S., Mandrioli, J., et al.; ITALSGEN Consortium (2009). Two Italian kindreds with familial amyotrophic lateral sclerosis due to FUS mutation. Neurobiol. Aging *30*, 1272–1275.

Devoy, A., Kalmar, B., Stewart, M., Park, H., Burke, B., Noy, S.J., Redhead, Y., Humphrey, J., Lo, K., Jaeger, J., et al. (2017). Humanized mutant FUS drives progressive motor neuron degeneration without aggregation in 'FUSDelta14' knockin mice. Brain *140*, 2797–2805.

Dormann, D., Rodde, R., Edbauer, D., Bentmann, E., Fischer, I., Hruscha, A., Than, M.E., Mackenzie, I.R., Capell, A., Schmid, B., et al. (2010). ALS-associated fused in sarcoma (FUS) mutations disrupt Transportin-mediated nuclear import. EMBO J. *29*, 2841–2857.

Dormann, D., Madl, T., Valori, C.F., Bentmann, E., Tahirovic, S., Abou-Ajram, C., Kremmer, E., Ansorge, O., Mackenzie, I.R., Neumann, M., and Haass, C. (2012). Arginine methylation next to the PY-NLS modulates Transportin binding and nuclear import of FUS. EMBO J. *31*, 4258–4275.

Edbauer, D., and Haass, C. (2016). An amyloid-like cascade hypothesis for C9orf72 ALS/FTD. Curr. Opin. Neurobiol. *36*, 99–106.

Elbaum-Garfinkle, S., Kim, Y., Szczepaniak, K., Chen, C.C., Eckmann, C.R., Myong, S., and Brangwynne, C.P. (2015). The disordered P granule protein LAF-1 drives phase separation into droplets with tunable viscosity and dynamics. Proc. Natl. Acad. Sci. USA *112*, 7189–7194.

Fuhrmann, J., Clancy, K.W., and Thompson, P.R. (2015). Chemical biology of protein arginine modifications in epigenetic regulation. Chem. Rev. *115*, 5413–5461.

Fujimura, K., Suzuki, T., Yasuda, Y., Murata, M., Katahira, J., and Yoneda, Y. (2010). Identification of importin alpha1 as a novel constituent of RNA stress granules. Biochim. Biophys. Acta *1803*, 865–871.

Göbl, C., Resch, M., Strickland, M., Hartlmüller, C., Viertler, M., Tjandra, N., and Madl, T. (2016). Increasing the Chemical-Shift Dispersion of Unstructured Proteins with a Covalent Lanthanide Shift Reagent. Angew. Chem. Int. Ed. Engl. *55*, 14847–14851.

Guo, L., Kim, H.J., Wang, H., Monaghan, J., Freyermuth, F., Sung, J., O'Donovan, K., Fare, C., Diaz, Z., Singh, N., et al. (2018). Nuclear-Import Receptors Reverse Aberrant Phase Transitions of RNA-Binding Proteins with Prion-like Domains. Cell *173*. Published online April 19, 2018. https://doi.org/10.1016/j.cell.2018.03.002.

Hutten, S., Flotho, A., Melchior, F., and Kehlenbach, R.H. (2008). The Nup358-RanGAP complex is required for efficient importin alpha/beta-dependent nuclear import. Mol. Biol. Cell *19*, *2300–*2310.

Jäkel, S., Mingot, J.M., Schwarzmaier, P., Hartmann, E., and Görlich, D. (2002). Importins fulfil a dual function as nuclear import receptors and cytoplasmic chaperones for exposed basic domains. EMBO J. *21*, 377–386.

Kato, M., Han, T.W., Xie, S., Shi, K., Du, X., Wu, L.C., Mirzaei, H., Goldsmith, E.J., Longgood, J., Pei, J., et al. (2012). Cell-free formation of RNA granules: low complexity sequence domains form dynamic fibers within hydrogels. Cell *149*, 753–767.

Kim, H.J., Kim, N.C., Wang, Y.D., Scarborough, E.A., Moore, J., Diaz, Z., MacLea, K.S., Freibaum, B., Li, S., Molliex, A., et al. (2013). Mutations in prion-like domains in hnRNPA2B1 and hnRNPA1 cause multisystem proteinopathy and ALS. Nature *495*, 467–473.

King, O.D., Gitler, A.D., and Shorter, J. (2012). The tip of the iceberg: RNA-binding proteins with prion-like domains in neurodegenerative disease. Brain Res. *1462*, 61–80.

Kosugi, S., Hasebe, M., Entani, T., Takayama, S., Tomita, M., and Yanagawa, H. (2008). Design of peptide inhibitors for the importin alpha/beta nuclear import pathway by activity-based profiling. Chem. Biol. *15*, 940–949.

Kwiatkowski, T.J., Jr., Bosco, D.A., Leclerc, A.L., Tamrazian, E., Vanderburg, C.R., Russ, C., Davis, A., Gilchrist, J., Kasarskis, E.J., Munsat, T., et al. (2009). Mutations in the FUS/TLS gene on chromosome 16 cause familial amyotrophic lateral sclerosis. Science *323*, 1205–1208.

Lee, B.J., Cansizoglu, A.E., Süel, K.E., Louis, T.H., Zhang, Z., and Chook, Y.M. (2006). Rules for nuclear localization sequence recognition by karyopherin beta 2. Cell *126*, 543–558.

Lee, K.H., Zhang, P., Kim, H.J., Mitrea, D.M., Sarkar, M., Freibaum, B.D., Cika, J., Coughlin, M., Messing, J., Molliex, A., et al. (2016). C9orf72 Dipeptide Repeats Impair the Assembly, Dynamics, and Function of Membrane-Less Organelles. Cell *167*, 774–788.

Li, Y.R., King, O.D., Shorter, J., and Gitler, A.D. (2013). Stress granules as crucibles of ALS pathogenesis. J. Cell Biol. *201*, 361–372.

Lin, Y., Currie, S.L., and Rosen, M.K. (2017). Intrinsically disordered sequences enable modulation of protein phase separation through distributed tyrosine motifs. J. Biol. Chem. *292*, 19110–19120.

Ling, S.C., Polymenidou, M., and Cleveland, D.W. (2013). Converging mechanisms in ALS and FTD: disrupted RNA and protein homeostasis. Neuron *79*, 416–438.

Livernois, A.M., Hnatchuk, D.J., Findlater, E.E., and Graether, S.P. (2009). Obtaining highly purified intrinsically disordered protein by boiling lysis and single step ion exchange. Anal. Biochem. *392*, 70–76.

Love, D.C., Sweitzer, T.D., and Hanover, J.A. (1998). Reconstitution of HIV-1 rev nuclear export: independent requirements for nuclear import and export. Proc. Natl. Acad. Sci. USA *95*, 10608–10613.

Mackenzie, I.R., Rademakers, R., and Neumann, M. (2010). TDP-43 and FUS in amyotrophic lateral sclerosis and frontotemporal dementia. Lancet Neurol. *9*, 995–1007.

Mackenzie, I.R., Nicholson, A.M., Sarkar, M., Messing, J., Purice, M.D., Pottier, C., Annu, K., Baker, M., Perkerson, R.B., Kurti, A., et al. (2017). TIA1 Mutations in Amyotrophic Lateral Sclerosis and Frontotemporal Dementia Promote Phase Separation and Alter Stress Granule Dynamics. Neuron *95*, 808–816.

Milles, S., Huy Bui, K., Koehler, C., Eltsov, M., Beck, M., and Lemke, E.A. (2013). Facilitated aggregation of FG nucleoporins under molecular crowding conditions. EMBO Rep. *14*, 178–183.

Molliex, A., Temirov, J., Lee, J., Coughlin, M., Kanagaraj, A.P., Kim, H.J., Mittag, T., and Taylor, J.P. (2015). Phase separation by low complexity domains promotes stress granule assembly and drives pathological fibrillization. Cell *163*, 123–133.

Mori, K., Lammich, S., Mackenzie, I.R., Forné, I., Zilow, S., Kretzschmar, H., Edbauer, D., Janssens, J., Kleinberger, G., Cruts, M., et al. (2013). hnRNP A3 binds to GGGGCC repeats and is a constituent of p62-positive/TDP43-negative inclusions in the hippocampus of patients with C9orf72 mutations. Acta Neuropathol. *125*, 413–423.

Murakami, T., Qamar, S., Lin, J.Q., Schierle, G.S., Rees, E., Miyashita, A., Costa, A.R., Dodd, R.B., Chan, F.T., Michel, C.H., et al. (2015). ALS/FTD Mutation-Induced Phase Transition of FUS Liquid Droplets and Reversible Hydrogels into Irreversible Hydrogels Impairs RNP Granule Function. Neuron *88*, 678–690.

Neumann, M., Sampathu, D.M., Kwong, L.K., Truax, A.C., Micsenyi, M.C., Chou, T.T., Bruce, J., Schuck, T., Grossman, M., Clark, C.M., et al. (2006). Ubiquitinated TDP-43 in frontotemporal lobar degeneration and amyotrophic lateral sclerosis. Science *314*, 130–133.

Neumann, M., Rademakers, R., Roeber, S., Baker, M., Kretzschmar, H.A., and Mackenzie, I.R. (2009). A new subtype of frontotemporal lobar degeneration with FUS pathology. Brain *132*, 2922–2931.

Neumann, M., Bentmann, E., Dormann, D., Jawaid, A., DeJesus-Hernandez, M., Ansorge, O., Roeber, S., Kretzschmar, H.A., Munoz, D.G., Kusaka, H., et al. (2011). FET proteins TAF15 and EWS are selective markers that distinguish FTLD with FUS pathology from amyotrophic lateral sclerosis with FUS mutations. Brain *134*, 2595–2609.

Neumann, M., Valori, C.F., Ansorge, O., Kretzschmar, H.A., Munoz, D.G., Kusaka, H., Yokota, O., Ishihara, K., Ang, L.C., Bilbao, J.M., and Mackenzie, I.R. (2012). Transportin 1 accumulates specifically with FET proteins but no other transportin cargos in FTLD-FUS and is absent in FUS inclusions in ALS with FUS mutations. Acta Neuropathol. *124*, 705–716.

Noegel, A.A., Blau-Wasser, R., Sultana, H., Müller, R., Israel, L., Schleicher, M., Patel, H., and Weijer, C.J. (2004). The cyclase-associated protein CAP as regulator of cell polarity and cAMP signaling in Dictyostelium. Mol. Biol. Cell *15*, 934–945.

Nott, T.J., Petsalaki, E., Farber, P., Jervis, D., Fussner, E., Plochowietz, A., Craggs, T.D., Bazett-Jones, D.P., Pawson, T., Forman-Kay, J.D., and Baldwin, A.J. (2015). Phase transition of a disordered nuage protein generates environmentally responsive membraneless organelles. Mol. Cell *57*, 936–947.

Nott, T.J., Craggs, T.D., and Baldwin, A.J. (2016). Membraneless organelles can melt nucleic acid duplexes and act as biomolecular filters. Nat. Chem. *8*, 569–575.

Ong, S.E., Mittler, G., and Mann, M. (2004). Identifying and quantifying in vivo methylation sites by heavy methyl SILAC. Nat. Methods *1*, 119–126.

Orozco, D., Tahirovic, S., Rentzsch, K., Schwenk, B.M., Haass, C., and Edbauer, D. (2012). Loss of fused in sarcoma (FUS) promotes pathological Tau splicing. EMBO Rep. *13*, 759–764.

Ozdilek, B.A., Thompson, V.F., Ahmed, N.S., White, C.I., Batey, R.T., and Schwartz, J.C. (2017). Intrinsically disordered RGG/RG domains mediate degenerate specificity in RNA binding. Nucleic Acids Res. *45*, 7984–7996.

Patel, A., Lee, H.O., Jawerth, L., Maharana, S., Jahnel, M., Hein, M.Y., Stoynov, S., Mahamid, J., Saha, S., Franzmann, T.M., et al. (2015). A Liquid-to-Solid Phase Transition of the ALS Protein FUS Accelerated by Disease Mutation. Cell *162*, 1066–1077.

Ryan, V.H., Dignon, G.L., Zerze, G.H., Chabata, C.V., Silva, R., Conicella, A.E., Amaya, J., Burke, K.A., Mittal, J., and Fawzi, N.L. (2018). Mechanistic View of hnRNPA2 Low-Complexity Domain Structure, Interactions, and Phase Separation Altered by Mutation and Arginine Methylation. Mol. Cell *69*, 465–479.

Saha, S., Weber, C.A., Nousch, M., Adame-Arana, O., Hoege, C., Hein, M.Y., Osborne-Nishimura, E., Mahamid, J., Jahnel, M., Jawerth, L., et al. (2016). Polar Positioning of Phase-Separated Liquid Compartments in Cells Regulated by an mRNA Competition Mechanism. Cell *166*, 1572–1584.

Scaramuzzino, C., Monaghan, J., Milioto, C., Lanson, N.A., Jr., Maltare, A., Aggarwal, T., Casci, I., Fackelmayer, F.O., Pennuto, M., and Pandey, U.B. (2013). Protein arginine methyltransferase 1 and 8 interact with FUS to modify its subcellular distribution and toxicity in vitro and in vivo. PLoS ONE *8*, e61576.

Scekic-Zahirovic, J., Oussini, H.E., Mersmann, S., Drenner, K., Wagner, M., Sun, Y., Allmeroth, K., Dieterlé, S., Sinniger, J., Dirrig-Grosch, S., et al. (2017). Motor neuron intrinsic and extrinsic mechanisms contribute to the pathogenesis of FUS-associated amyotrophic lateral sclerosis. Acta Neuropathol. *133*, 887–906.

Schindelin, J., Arganda-Carreras, I., Frise, E., Kaynig, V., Longair, M., Pietzsch, T., Preibisch, S., Rueden, C., Saalfeld, S., Schmid, B., et al. (2012). Fiji: an open-source platform for biological-image analysis. Nat. Methods *9*, 676–682.

Schwartz, J.C., Wang, X., Podell, E.R., and Cech, T.R. (2013). RNA seeds higher-order assembly of FUS protein. Cell Rep. *5*, 918–925.

Snowden, J.S., Hu, Q., Rollinson, S., Halliwell, N., Robinson, A., Davidson, Y.S., Momeni, P., Baborie, A., Griffiths, T.D., Jaros, E., et al. (2011). The most common type of FTLD-FUS (aFTLD-U) is associated with a distinct clinical form of frontotemporal dementia but is not related to mutations in the FUS gene. Acta Neuropathol. *122*, 99–110.

Suárez-Calvet, M., Neumann, M., Arzberger, T., Abou-Ajram, C., Funk, E., Hartmann, H., Edbauer, D., Kremmer, E., Göbl, C., Resch, M., et al. (2016). Monomethylated and unmethylated FUS exhibit increased binding to Transportin and distinguish FTLD-FUS from ALS-FUS. Acta Neuropathol. *131*, 587–604.

Sun, Z., Diaz, Z., Fang, X., Hart, M.P., Chesi, A., Shorter, J., and Gitler, A.D. (2011). Molecular determinants and genetic modifiers of aggregation and toxicity for the ALS disease protein FUS/TLS. PLoS Biol. *9*, e1000614.

Taylor, J.P., Hardy, J., and Fischbeck, K.H. (2002). Toxic proteins in neurodegenerative disease. Science *296*, 1991–1995.

Thandapani, P., O'Connor, T.R., Bailey, T.L., and Richard, S. (2013). Defining the RGG/RG motif. Mol. Cell *50*, 613–623.

van den Bogaart, G., Meinema, A.C., Krasnikov, V., Veenhoff, L.M., and Poolman, B. (2009). Nuclear transport factor directs localization of protein synthesis during mitosis. Nat. Cell Biol. *11*, 350–356.

Vance, C., Rogelj, B., Hortobágyi, T., De Vos, K.J., Nishimura, A.L., Sreedharan, J., Hu, X., Smith, B., Ruddy, D., Wright, P., et al. (2009). Mutations in FUS, an RNA processing protein, cause familial amyotrophic lateral sclerosis type 6. Science *323*, 1208–1211.

Weinmann, L., Höck, J., Ivacevic, T., Ohrt, T., Mütze, J., Schwille, P., Kremmer, E., Benes, V., Urlaub, H., and Meister, G. (2009). Importin 8 is a gene silencing factor that targets argonaute proteins to distinct mRNAs. Cell *136*, 496–507.

Wiśniewski, J.R., Hein, M.Y., Cox, J., and Mann, M. (2014). A "proteomic ruler" for protein copy number and concentration estimation without spike-in standards. Mol. Cell. Proteomics *13*, 3497–3506.

Yang, Y., and Bedford, M.T. (2013). Protein arginine methyltransferases and cancer. Nat. Rev. Cancer *13*, 37–50.

Yoneda, Y., Imamoto-Sonobe, N., Yamaizumi, M., and Uchida, T. (1987). Reversible inhibition of protein import into the nucleus by wheat germ agglutinin injected into cultured cells. Exp. Cell Res. *173*, 586–595.

Yoshizawa, T., Ali, R., Jiou, J., Fung, H.Y.J., Burke, K.A., Kim, S.J., Lin, Y., Peeples, W.B., Saltzberg, D., Soniat, M., et al. (2018). Nuclear Import Receptor Inhibits Phase Separation of FUS through Binding to Multiple Sites. Cell *173*. Published online April 19, 2018. https://doi.org/10.1016/j.cell.2018.03.003.

Zhang, X., and Cheng, X. (2003). Structure of the predominant protein arginine methyltransferase PRMT1 and analysis of its binding to substrate peptides. Structure *11*, 509–520.

Zhang, Z.C., and Chook, Y.M. (2012). Structural and energetic basis of ALS-causing mutations in the atypical proline-tyrosine nuclear localization signal of the Fused in Sarcoma protein (FUS). Proc. Natl. Acad. Sci. USA *109*, 12017–12021.

STAR★METHODS

KEY RESOURCES TABLE

REAGENT or RESOURCE	SOURCE	IDENTIFIER
Antibodies		
FUS (4H11)	Santa Cruz	RRID:AB_2105208
UMA FUS (14G1)	D.D.; Suárez-Calvet et al., 2016	N/A
MMA FUS (15E11)	D.D.; Suárez-Calvet et al., 2016	N/A
ADMA FUS (9G6)	D.D.; Dormann et al., 2012	N/A
G3BP1	Proteintech	RRID:AB_2232034
GFP (K3-184-2)	A. Noegel; Noegel et al., 2004	N/A
RFP	Thermo	RRID:AB_2315269
TIA-1	Santa Cruz	RRID:AB_2201433
Alexa 555 Donkey anti-rabbit	Thermo	RRID:AB_162543
Alexa 647 Donkey anti-rabbit	Thermo	RRID:AB_2536183
Alexa 647 Donkey anti-goat	Thermo	RRID:AB_2535864
IRDye 680RD Donkey anti-Mouse IgG	LI-COR	RRID:AB_10953628
IRDye 680RD Goat anti-Rat IgG	LI-COR	RRID:AB_10956590
IRDye 800CW Donkey anti-Mouse IgG	LI-COR	RRID:AB_621847
Chemicals, Peptides, and Recombinant Proteins		
AcTEV Protease	Thermo	Cat# 12575015
GST-Precission	M. Geyer	N/A
Benzonase Nuclease	Sigma	Cat# E1014
Importin 5	D. Görlich; Jäkel et al., 2002	N/A
S-(5′-Adenosyl)-L-methionine *p*-toluenesulfonate	Sigma	Cat# A2408
TEM grids, carbon film coated, approx. 5-6 nm, 400 Mesh, Cu	Science Services	Cat# ECF400-Cu-25
4% Uranyl Acetate Solution	Science Services	Cat# E22400-4
[γ32P]ATP	Hartmann Analytic	Cat# SRP-401
DMEM, high glucose, GutaMAX supplement	Thermo	Cat# 61965059
Fetal Bovine Serum, qualified, heat inactivated, E.U.-approved, South America Origin	Thermo	Cat# 10500064
Fetal Bovine Serum, dialyzed, US origin	Thermo	Cat# 26400044
Gentamicin (10 mg/mL)	Thermo	Cat# 15710049
TurboFect Transfection Reagent	Thermo	Cat# R0534
Aprotinin	Roth	Cat# A162
Leupeptin hemisulfate	Roth	Cat# CN33
Pepstatin A	Roth	Cat# 2936
Lectin from Triticum vulgaris (Wheat germ agglutinin, WGA)	Sigma	Cat# L9640
Digitonin	Calbiochem	Cat# 300410
ProLong Diamond Antifade Mountant	Thermo	Cat# P36965
DAPI	Sigma	Cat# D9542
Poly-L-Lysine	Sigma	Cat# P9155
Sypro-Ruby Protein Gel Stain	Sigma	Cat# S4942
Bacterial and Virus Strains		
BL21-Codon Plus (DE3)-RIPL	Agilent Technologies	Cat# 230280
BL21-DE3-Rosetta-LysS	D. Niessing	N/A

(*Continued on next page*)

Continued

REAGENT or RESOURCE	SOURCE	IDENTIFIER
BL21-DE3 Rosetta	C. Haass	N/A
BL21-DE3	Agilent Technologies	Cat# 200131
Experimental Models: Cell Lines		
HeLa P4	R. Kehlenbach; Charneau et al., 1994	N/A
HeLa Kyoto	I. Poser and A. Hyman	RRID: CVCL_1922
Recombinant DNA		
pMal-*Tev*-Flag-FUS-*Tev*-His_6	This paper	N/A
pMal-*Tev*-FUS (WT)-EGFP-*Tev*-His_6	This paper	N/A
pMal-*Tev*-FUS (P525L)-EGFP-*Tev*-His_6	This paper	N/A
pMal-C2-*Tev*-Flag-FUS-ΔRGG3-PY-*Tev*-His_6	This paper	N/A
pMal-C2-*Tev*-Flag-FUS-all-KGG-*Tev*-His_6	This paper	N/A
pEX-A2-linker-EGFP-His_6	This paper, IDT	N/A
petM11-His_6-ZZ-*Tev*-FUS-RGG3-PY (WT and P525L)	D.D.; Dormann et al., 2012	N/A
petM11-His_6-ZZ-*Tev*-FUS-KGG3-PY	This paper	N/A
petM11-His_6-ZZ-*Tev*-TNPO1	T.M.; Suárez-Calvet et. al., 2016	N/A
pET28b-PRMT1	E. Wahle; Zhang and Cheng, 2003	N/A
His_6-TEV in a pET-24d(+) vector	A. Geerlof	N/A
pEGFP-bimax	D.D.; Dormann et al., 2010	N/A
pRSV-EGFP-M9M	This paper	N/A
GCR_2-tagRFP$_2$-FUS WT	This paper	N/A
GCR_2-tagRFP$_2$-FUS P525L	This paper	N/A
pGM3 mTaul9-28560	D. Edbauer, Orozco et al., 2012	N/A
Oligonucleotides		
Primers for PCR, see Table S3	This paper	N/A
Oligonucleotides, see Table S3	This paper	N/A
Software and Algorithms		
ImageJ (Fiji)	NIH, Schindelin et al., 2012	RRID:SCR_003070
Image Studio Lite	Li-COR	RRID:SCR_014211
Zen2 blue edition (lite)	Zeiss	RRID:SCR_013672
LAS X	Leica	RRID:SCR_013673
GraphPad Prism5	GraphPad Software	RRID:SCR_002798
PONDR® VL-XT	Molecular Kinetics, Washington State University; WSU Research Foundation	http://www.pondr.com/
TEM Center Software	JEOL	N/A
Sight X Viewer Software	JEOL	N/A
Origin	OriginLab	RRID:SCR_014212
TopSpin 3.1	Bruker	RRID:SCR_014227

CONTACT FOR REAGENT AND RESOURCE SHARING

Further information and requests for reagents may be directed to and will be fulfilled by the Lead Contact, Dorothee Dormann (dorothee.dormann@med.uni-muenchen.de)

EXPERMENTAL MODEL AND SUBJECT DETAILS

Cell culture and transfection

HeLa Kyoto cells for transient transfection experiments and HeLa-P4 cells (Charneau et al., 1994) for semi-permeabilized cell assays were grown in DMEM high glucose GlutaMAX (Invitrogen) supplemented with 10% dialyzed FBS, or 10% standard FBS and 10 μg/ml gentamicin, respectively. Cells were maintained in a humidified incubator at 37°C with 5% CO_2. Transient transfections were

performed using Turbofect following manual instructions. Note, that for transfection of GCR_2-tagRFP$_2$-FUS constructs low DNA amounts (20% GCR_2-tagRFP$_2$-FUS, 80% plasmid coding for EGFP/EGFP-bimax/EGFP-M9M) to minimize aggregation of FUS due to overexpression.

Bacterial Growth

All bacterial cultures were grown at 37°C under constant shaking (140-160 rpm) in standard lysogeny broth (LB) medium. Before induction of protein expression, cultures were cooled down to the temperature indicated for the respective protein in the section "Recombinant protein expression and purification."

METHOD DETAILS

Generation of cDNA constructs

pMal-*Tev*-Flag-FUS-*Tev*-His$_6$ was created by cloning PCR amplified N-terminal Flag-tagged and C-terminal *Tev*-His$_6$ tagged FUS cDNA into the SalI-HindIII sites of pMal-*Tev* using primers SalI_flag_F and HindIII_His$_6$-*Tev*-FUS_R. pMal-*Tev* was created by cloning annealed double stranded oligonucleotides *Tev*_F and *Tev*_R (coding for the *Tev* cleavage site) into the EcoRI-SalI sites of pMal-c.

To generate pMal-*Tev*-FUS-EGFP-*Tev*-His$_6$, FUS cDNA was PCR amplified from pMal-*Tev*-Flag-FUS-*Tev*-His$_6$ using primers SalI_FUS_F and BamHI_FUS_R, thus introducing a C-terminal BamHI restriction site. EGFP-His$_6$ with low-complexity linker was cut from synthetic pEX-A2-linker-EGFP-His$_6$ (IDT) using BamHI and HindIII sites. In a triple ligation, FUS and EGFP-His$_6$ fragments were cloned into the pMal-*Tev* backbone derived from pMal-*Tev*-flag-FUS-*Tev*-His$_6$.

pMal-*Tev*-FUS (P525L)-EGFP-*Tev*-His$_6$ was generated by site directed mutagenesis of pMal-*Tev*-FUS-EGFP-*Tev*-His$_6$ using primers FUS wt-EGFP mut P525L_F and FUS wt-EGFP mut P525L_R.

To generate pMal-C2-Tev, the C terminus of MBP including parts of the MCS was PCR-amplified (MBP_NcoI_F; MBPLinker_Tev_EcoRI) introducing a Tev-cleavage site in the reverse primer and replacing the factor Xa cleavage site in the original pMal-C2 (NEB) vector.

pMal-C2-*Tev*-Flag-FUS ΔRGG3-PY-*Tev*-His$_6$ was generated by cloning PCR amplified N-terminal Flag-tagged and C-terminal *Tev*-His$_6$ tagged FUS cDNA encoding amino acids 1-453 into the SalI-HindIII sites of pMal-C2-*Tev* using primers SalI_flag_F and HindIII_FUS453X-*Tev*-His$_6$_R.

To generate pMal-C2-*Tev*-Flag-FUS-all-KGG-*Tev*-His$_6$, FUS cDNA was PCR amplified from a synthetic plasmid with all RGGs mutated to KGGs using primers XhoI_FUS_F and HindIII_*Tev*-His$_6$- -FUS_R and cloned into the pMal-C2-*TEV* backbone derived from pMal-C2-*Tev*-Flag-FUS ΔRGG3-PY-*Tev*-His$_6$.

petM11-His$_6$-ZZ-*Tev*-FUS-KGG3-PY was generated by cloning FUS cDNA encoding amino acids 454-526 from a synthetic plasmid with all RGGs mutated to KGGs using primers FUS 454_NcoI_F and BamHI_FUS_R and cloned into the petM11-His$_6$-ZZ backbone derived from petM11-His$_6$-ZZ-*Tev*-FUS-RGG3-PY.

To generate pETM11-His$_6$-ZZ-*Tev*-TNPO1, the human TNPO1 cDNA sequence was codon optimized for protein production in bacterial cells and flanked by NcoI and BamHI restriction sites (Genscript). The coding region was cloned into a modified pETM11 bacterial expression vector, which includes an N-terminal His$_6$, protein A (ZZ) tag and a TEV protease cleavage site.

To generate GCR_2-tagRFP$_2$-FUS, the EGFP$_2$-sequence in a modified EGFP-C1 vector containing a GCR_2-EGFP$_2$-cassette (Hutten et al., 2008) was replaced sequentially with a two cDNAs coding for tagRFP (primer: TagRFP_AgeI/TagRFP_EcoRV and TagRFP_Spe/ TagRFP_AgeI_R). FUS wt or P525L was inserted via EcoRV/BamHI sites replacing the NLS sequence (primer: FUS_EcoRV_f with either FUS_BamHI_R or FusP525L_BamHIr).

The pRSV-EGFP-M9M construct was generated by replacing the CMV-promoter in pEGFP-M9M (Dormann et al., 2010) by a RSV promoter sequence (gift from M. Kiebler) via AseI/NheI.

Recombinant protein expression and purification

For expression of recombinant MBP-FUS-His$_6$ (WT, ΔRGG3-PY, and all-KGG) and MBP-FUS-EGFP-His$_6$ (WT and P525L), the respective bacterial expression vectors were transformed into *E. coli* BL21-DE3-RIPL and BL21-DE3-Rosetta-LysS, respectively, and grown in standard lysogeny broth (LB) medium. At an OD (600 nm) of ~0.8, cells were induced with 0.1 mM IPTG for 22 h at 12°C. Cells were lysed in resuspension buffer (50 mM Na_2HPO_4/NaH_2PO_4, pH 8.0, 300 mM NaCl, 10 μM $ZnCl_2$, 40 mM imidazole, 4 mM βME) + 10% glycerol and tandem-affinity purification using HisTrap FF columns (GE Healthcare) and amylose resin (NEB) was performed. The protein was washed with resuspension buffer and eluted in resuspension buffer including 250 mM imidazole and 20 mM maltose, respectively.

For expression of recombinant His$_6$-Tev, *E. coli* BL21-Ros-LysS were transformed with the expression plasmid and grown in standard LB medium. Induction of expression was induced at OD (600 nm) of ~0.6 with 1mM IPTG overnight at 20°C. Cells were lysed in lysis buffer (50 mM Tris pH8, 200 mM NaCl, 20 mM imidazole, 10% glycerol, 4 mM β-mercaptoethanol, 1 μg/ml each of aprotinin, leupeptin and pepstatin) by addition of lysozyme and sonification. The lysate was incubated in the presence of RNase A (0.1mg/ml final concentration) for 30min at RT. His-Tev was purified using Ni-NTA beads and washed using lysis buffer containing 1M NaCl. His$_6$-Tev was eluted in lysis buffer (pH 8.5) containing 800mM imidazole and dialyzed against storage buffer (20mM Tris pH 7.4; 150mM NaCl; 20% glycercole, 2mM DTT).

For expression of the RGG3-PY domain, pETM11-His_6-ZZ-FUS-RGG3-PY (WT and KGG3-PY) were transformed into *E. coli* BL21-DE3 Rosetta and were expressed at 37°C for 4 h. Cells in resuspension buffer were lysed by boiling for 20 min at 90°C, as boiling lysis allows removal of folded proteins from cell lysates, while intrinsically disordered proteins stay soluble (Livernois et al., 2009). His_6-ZZ tagged proteins were bound to nickel-nitrilotiacetic (Ni-NTA) resin (QIAGEN), incubated with Benzonase Nuclease (Sigma) overnight at 4°C in Benzonase buffer (50 mM Na_2HPO_4/NaH_2PO_4, pH 8.0, 50 mM NaCl, 2 mM $MgCl_2$) and subjected to high salt washes with resuspension buffer containing 2 M NaCl and then eluted in resuspension buffer + 250 mM imidazole. In order to proteolytically remove the His_6-ZZ tag, His_6-TEV protease (2.5 mg) was added to eluted His_6-ZZ-RGG3-PY proteins and dialyzed against *TEV* cleavage buffer (20 mM Na_2HPO_4/NaH_2PO_4, pH 8.1, 150 mM NaCl, 5% glycerol, 4 mM βME) overnight at 4°C. His_6-TEV and His_6-ZZ tag were removed by incubation with Ni-NTA resin (QIAGEN), while untagged RGG3-PY remains in the supernatant.

For ITC or NMR experiments, pETM11-His_6-ZZ-FUS-RGG3-PY (WT or P525L) were transformed into *E. coli* BL21-DE3 Star strain. For the unlabeled protein, cells were grown for 1 day at 37°C in standard lysogeny broth (LB) medium. At an OD (600 nm) of ~0.8, cells were induced with 0.1 mM IPTG for 22 h at 12°C. To obtain ^{15}N labeled protein, cells were grown for 1 day at 37°C in minimal medium (100 mM KH_2PO_4, 50 mM K_2HPO_4, 60 mM Na_2HPO_4, 14 mM K_2SO_4, 5 mM $MgCl_2$; pH 7.2 adjusted with HCl and NaOH with 0.1 dilution of trace element solution (41 mM $CaCl_2$, 22 mM $FeSO_4$, 6 mM $MnCl_2$, 3 mM $CoCl_2$, 1 mM $ZnSO_4$, 0.1 mM $CuCl_2$, 0.2 mM $(NH_4)_6Mo_7O_{24}$, 17 mM EDTA) supplemented with 6 g of $^{12}C_6H_{12}O_6$ and 1 g of $^{15}NH_4Cl$ (Sigma). At an OD (600 nm) of ~0.8, cells were induced with 0.5 mM IPTG for 16 h at 20°C. Cell pellets were harvested and sonicated in denaturing buffer containing 50mM Tris-HCl pH 7.5, 150 mM NaCl, 20 mM imidazole, 2 mM tris(2-carboxyethyl)phosphine (TCEP), 20% glycerol and 6M urea. His_6-ZZ proteins were purified using Ni-NTA agarose (QIAGEN) and eluted in 50 mM Tris-HCl pH 7.5, 150 mM NaCl, 200 mM imidazole, 2 mM TCEP and subjected to TEV treatment. Untagged proteins were then isolated performing a second affinity purification using Ni-NTA beads. A final exclusion chromatography purification step was performed in the buffer of interest on a gel filtration column (Superdex peptide, GE Healthcare).

For expression of recombinant His_6-TNPO1, the bacterial expression vector pETM11-His_6-ZZ-*Tev*-TNPO1 was transformed into *E. coli* BL21-DE3 Star cells. Expression cultures of 1 l volume were grown for 2 days in minimal medium (100 mM KH_2PO_4, 50 mM K_2HPO_4, 60 mM Na_2HPO_4, 14 mM K_2SO_4, 5 mM $MgCl_2$; pH 7.2 adjusted with HCl and NaOH with 0.1 dilution of trace element solution (41 mM $CaCl_2$, 22 mM $FeSO_4$, 6 mM $MnCl_2$, 3 mM $CoCl_2$, 1 mM $ZnSO_4$, 0.1 mM $CuCl_2$, 0.2 mM $(NH_4)_6Mo_7O_{24}$, 17 mM EDTA) supplemented with 6 g of glucose and 3 g of NH_4Cl. Cells were diluted to an OD (600 nm) of 0.8 and induced with 0.5 mM IPTG followed by protein expression for 4 h at room temperature. His_6-TNPO1 was purified using Ni-NTA agarose (QIAGEN) and eluted in 50 mM Tris-HCl pH 7.5, 150 mM NaCl, 200 mM imidazole, 2 mM TCEP. A final size exclusion chromatography step was performed in 50 mM Tris-HCl pH 7.5, 150 mM NaCl, 20 mM imidazole, 2 mM TCEP, 20% glycerol on a gel filtration column (Hiload 16/600 Superdex 200 pg, GE Healthcare). Note, that for ITC/NMR experiments, the His-tag was removed by TEV cleavage.

For expression of recombinant His_6-PRMT1, the pET28b-PRMT1 vector was transformed into *E. coli* BL21-DE3 Star and 1 l expression culture was grown in LB medium. Cells were induced at an OD (600 nm) of 0.8 with 0.5 mM IPTG followed by protein expression for 16 h at 20°C. Cell pellets were harvested and sonicated in 50mM Tris-HCl pH 7.5, 150 mM NaCl, 20 mM imidazole, 2 mM TCEP, 20% glycerol. His_6-PRMT1 was purified using 5 mL HisTrap HP column (GE Healthcare), eluted in 50 mM Tris-HCl pH 7.5, 1 M NaCl, 500 mM imidazole, 2 mM TCEP and further purified by size exclusion chromatography as described for TNPO1 above.

Protein concentrations were determined from their absorbance at 280 nm using ε predicted by the ProtParam tool. For all assay that involved addition of RNA, 260/280 nm ratios of purified proteins were between 0.6 and 0.8.

In vitro methylation

FUS proteins and PRMT1 were dialyzed against *in vitro* methylation (IVM) buffer containing 20 mM Na_2HPO_4/NaH_2PO_4, pH 8.1, 150 mM NaCl, 5% glycerol, 1 mM EDTA, 1 mM DTT or 50 mM Na_2HPO_4/NaH_2PO_4, pH 8.0, 150 mM NaCl, 2 mM TCEP for ITC and NMR experiments. FUS proteins were *in vitro* methylated by incubating with PRMT1 and 1 mM S-adenosyl-L-methionine (SAM) overnight at room temperature. PRMT1 was used at a molar ratio of 2:1 for MBP-FUS, 1.5:1 for RGG3-PY or KGG3-PY (used in droplet and turbidity assays) and 0.2:1 for RGG-PY proteins used in ITC or NMR experiments. For RGG3-PY proteins, PRMT1 was removed by boiling the samples for 10 min at 90°C.

In vitro transcription

MAPT RNA and *ASH1* E3-51 RNA were produced by *in vitro* transcription (MEGAshortscript Kit; Ambion) using linearized pGM3 mTaqI9-28560 or primers P45 and P132, respectively.

For filter binding assays the *ASH1* RNA was radioactively labeled using [γ32P]ATP and T4 polynucleotide kinase (NEB). The RNA was separated from free nucleotides using NucAway spin columns (Ambion).

In vitro phase separation assays

Droplet assay for microscopy

Purified RGG3-PY or KGG3-PY and His_6-TNPO1 were buffer exchanged to droplet buffer (20 mM Na_2HPO_4/NaH_2PO_4, pH 7.5, 75 mM NaCl, 2.5% glycerol, 1 mM DTT) and concentrated in Amicon Ultra Centrifugal Filter Devices (Millipore). For droplet formation of C-terminal RGG3-PY proteins, proteins were diluted to indicated concentrations and supplemented with *in vitro* transcribed *MAPT*

RNA (a known FUS target RNA, Orozco et al., 2012) at a molar ratio of 1:50, as this ratio was found to maximally promote phase separation. His_6-TNPO1, His_6-Importin 5, αFUS RGG3, or His_6-PRMT1, respectively, were used at equimolar concentrations to FUS.

Purified full-length MBP-FUS-EGFP (WT or P525L) or MBP-FUS were diluted in droplet buffer including 150 mM NaCl, if not otherwise stated in the figure legend. Full-length FUS was only supplemented with RNA when explicitly mentioned in the figure legend (Figure 3G). Phase separation was induced by addition of acTEV protease (Invitrogen) at 25°C. With the exception of Figure 4A, where widefield fluorescence microscopy was applied, imaging of EGFP-tagged FUS was performed by confocal microscopy. Non-fluorescent FUS-droplets were imaged by phase contrast microscopy.

Note that phase separation properties, i.e., critical concentration for droplet formation, differ slightly between different protein preparations.

In vitro aging assay

To induce aging of FUS-EGFP droplets, TEV-cleaved samples were subjected to 700 rpm on an orbital shaker at RT for 8h and additionally mixed by pipetting up and down every hour. Samples were imaged in 384-well plates by confocal microscopy.

Turbidity assay

Phase separation of RGG3-PY and MBP-FUS in the absence or presence of equimolar amounts of His_6-TNPO1, His_6-Importin 5, αFUS RGG3, or His_6-PRMT1, respectively, was induced as described above for the droplet assay. Turbidity measurements were conducted at 600 nm in 384-well plates with 20 μl samples using a BioTek Power Wave HT plate reader. All experiments were performed in triplicate.

Sedimentation assay

For sedimentation analysis of full-length FUS, the MBP-tag of 1 μM purified MBP-Flag-FUS protein in the absence or presence of equimolar amounts of His_6-TNPO1, His_6-Importin 5, αFUS RGG3, or His_6-PRMT1, respectively, was cleaved using 0.1 mg/ml His_6-TEV in 50 μl reaction buffer (50 mM Tris pH 8, 0.5 mM EDTA, 1 mM DTT) for 60 min at 30°C, followed by centrifugation at room temperature for 15 min at 16,000-20,000 g. Equal volumes of supernatant and pellet fraction were analyzed by SDS-PAGE and either SyproRuby stain (Figures 3D and S3C) or Western Blot with a FUS-specific antibody (4H11) (Figure 1D).

Semi-permeabilized cell assay

HeLa P4 cells were grown on poly-L-lysine coated 12 mm coverslips, permeabilized with 0.003%–0.005% digitonin in KPB (20 mM potassium phosphate pH 7.4, 250 mM sucrose, 5 mM $Mg(OAc)_2$, 200 mM KOAc, 1 mM EGTA, 2 mM DTT and 1μg/ml each aprotinin, pepstatin and leupeptin). After several washes to remove soluble proteins (4 × 4 min in KPB on ice), nuclear pores were blocked by 15 min incubation with 200 μg/ml wheat germ agglutinin (WGA) on ice. Cells were then incubated for 30 minutes at room temperature with 125 nM MBP-FUS-EGFP in the absence or presence of 1.25 μM His_6-TNPO1 in KPB. Note that a 10-fold excess of TNPO1 was required for efficient shielding of FUS, possibly due to other RBPs present in SGs that bind to TNPO1. Subsequently, cells were washed (3 × 5 min in KPB on ice) to remove unbound MBP-FUS-EGFP. SGs were visualized by immunostaining of G3BP1. Note that G3BP1 immunostaining also served as a control for proper permeabilization, as non/poorly-permeabilized cells still show diffuse cytoplasmic G3BP1 staining. Cells were imaged by confocal microscopy using identical settings for reactions within the same experiment.

Filter binding assay

The indicated protein concentrations were incubated with 0.5 nM of *in vitro* transcribed, radiolabeled *ASH1* E3-51 RNA in a total volume of 80 μL in filter-binding buffer (20 mM Na phosphate, 50 mM NaCl, 2 mM DTT, pH 7.5). Samples were applied to nitrocellulose and nylon membranes, using a Dot Blot Aparatus (BioRad), and washed twice with 80 μl filter-binding buffer. Membranes were air-dried and analyzed by phosphorimaging using a Fujifilm FLA-3000 scanner.

Immunocytochemistry

Cells grown on coverslips were either fixed ~20 h after transfection or after the semi-permeabilized cell assay in 3.7% formaldehyde/PBS buffer for 7-10 min at RT and permeabilized in 0.5% TX-100/ PBS for 5 min at room temperature. Cells were blocked for 10 min in blocking buffer (1% donkey serum in PBS/ 0.1% Tween-20) and incubated with primary antibodies in blocking buffer for 1-2h at RT or overnight at 4°C. Secondary antibodies were diluted in blocking buffer and incubated for 1h at room temperature. Washing steps after antibody incubation were performed with PBS/0.1% Tween-20. DNA was stained with DAPI at 0.5 μg/ml in PBS and cells mounted in ProLong Diamond Antifade. Imaging was performed by confocal microscopy.

Microscopy

Phase contrast and wide-field fluorescence microscopy

For imaging of FUS droplets, samples were placed in sealed sample chambers formed by a hole punched into a double-sided sticky tape, taped onto a glass slide and sealed with a coverslip.

For imaging of RGG3-PY and FUS droplets by phase contrast microscopy, a 63x/1.40 Oil/Ph3 objective was used; FUS-EGFP droplets in Figure 4A were imaged by fluorescence microscopy using a 63x/1.40 Oil objective, both on an Axio Oberver.Z1 wide-field fluorescence microscope and an AxioCam 506 (Zeiss, Oberkochen, Germany).

Confocal microscopy

Confocal microscopy was performed at the Bioimaging core facility of the Biomedical Center with an inverted Leica SP8 microscope, equipped with lasers for 405, 488, 552 and 638 nm excitation. Images were acquired using two-fold frame averaging with a 63x1.4 oil objective, and an image pixel size of 71 nm or 59 nm for droplets and cells, respectively. The following fluorescence settings were used for detection: DAPI: 419-442 nm, GFP: 498-533 nm, RFP/Alexa 555: 562-598 nm, Alexa 647: 650-700 nm. If applicable, recording was performed sequentially to avoid bleed-through using a conventional photomultiplier tube.

FRAP

In contrast to all other experiments in this study, droplet buffer including 75 mM NaCl was supplemented with 150 mg/ml Ficoll 400 in order to obtain droplets of similar size and shape for FRAP experiments. Experiments were performed on an inverted microscope (Axio Observer.Z1; Carl Zeiss, Oberkochen, Germany) equipped with a confocal spinning disk unit (CSU-X1; Yokogawa, Tokyo, Japan) and a Zeiss 100x/1.46 Oil Ph3 oil immersion lens. Images were acquired in the streaming mode using the 488 nm SD laser line and fixed exposure times of 50 ms and an EM-CCD camera (EvolveDelta; Photomoetrics) at bin 1x1. For localized photobleaching (“half-bleach”), a laser scanning device (UGA-42 Geo; Rapp OptoElectronic, Hamburg, Germany) was used. The “Geo” module allowed for simultaneous laser illumination within hardware-defined shapes of different sizes. Here, a square-like shape with an illumination size of $\sim$4 μm in the sample was selected. For each experiment, half of the observed structure was bleached to approximately 50% of the initial intensity using a 473 nm diode laser (DL-473/75; Rapp OptoElectronic, Hamburg, Germany).

Transmission electron microscopy (TEM)

Carbon coated copper grids (carbon film coated 400 mesh copper grids, Science Services) were glow discharged for 2 min in a Harrick plasma cleaner (PDC-32G-2) to facilitate protein adsorption. MBP-FUS (7 μM) -/+ TNPO1 (7 μM) was incubated with TEV protease for 90 min and subsequently diluted to 2 μM and deposited on the grid surface. The grid was washed twice in a drop of double distilled water, blotted shortly using filter paper. Fixing the grid by inverse forceps, 3 μl of 1% uranyl acetate were added to the grid for 30 s. After blotting, the grid was air-dried for at least 30 min. Mosaics of three by three images were obtained at a magnification of 60.000 using a JEOL JEM 1400-plus electron microscope at 120 kV (TEM Center software, JEOL). The Sight X Viewer (JEOL) and ImageJ (NIH) Software packages were applied for mosaic stitching.

Nuclear magnetic resonance

All proteins / RNA samples were prepared in 20 mM Na_2HPO_4/NaH_2PO_4 pH 7.5, 75 mM NaCl, 2.5% glycerol, 1 mM DTT and 10% ^2H_2O added for the lock signal. NMR experiments were performed at 25°C on Bruker 700 MHz spectrometer. Spectra were processed using Topspin 3.5 and Mnova 11.

Isothermal Calorimetry

All protein samples were prepared either in 50 mM Tris-HCl (pH 7.5), 150 mM NaCl and 2 mM tris(2-carboxyethyl)phosphine (TCEP) or in 50 mM Tris-HCl (pH 7.5), 1 M NaCl and 2 mM TCEP. ITC measurements were carried out on a MicroCal VP-ITC instrument (Microcal, Northhampton, USA) with 36 rounds of 8 μL injections at 25°C. Integration of peaks corresponding to each injection, subtraction of the contribution of protein dilution and correction for the baseline were performed using the Origin-based 7.0 software provided by the manufacturer. Curve fitting was done with a standard one-site model and gives the equilibrium binding constant (*Ka*), and enthalpy of the complex formation (ΔH).

QUANTIFICATION AND STATISTICAL ANALYSIS

Statistics

Statistical analyses were performed in GraphPad Prism 5. For 2-grouped analyses, for which control and treatment groups were handled in parallel, a paired t test was applied. If measurements were not normally distributed, a non-parametric test (Mann-Whitney) was chosen. 1-way ANOVAs were applied to multi-group comparisons. Here, a Bonferroni post-test was applied when significance between all groups was analyzed, whereas a Dunnett’s multiple comparison test was applied when the significance of all values to a single condition was analyzed.

Image analysis

Confocal images were acquired using LAS X (Leica), all other images were acquired in ZEN2 (Zeiss). For illustration of FRAP of FUS-EGFP droplets, images were displayed as heatmap and processed using the interpolation function in ZEN2. All other images were processed using ImageJ/Fiji software applying linear enhancement for brightness and contrast. For quantitative measurements, equal exposure times and processing conditions for respective channels were applied to all samples within one experiment. For better visibility, in some figures the individual channels were displayed in artificial colors as indicated in the figure legends.

Droplet quantification

Confocal images were imported in the public-domain software ImageJ/Fiji (Schindelin et al., 2012) and a Median filter with radius 2 was applied. Huang auto threshold method providing best coverage of the droplet area was applied. Structures touching the edge of the image section and/or smaller than 0.5 μm^2 were excluded from particle analysis. If required, a watershed analysis was performed.

Quantification of MBP-FUS-EGFP in SGs

For quantitative measurements, equal exposure times and processing conditions for respective channels were applied to all samples within one experiment. In ImageJ/Fiji, ROIs corresponding to SGs were identified using the wand tool by G3BP1 staining and mean fluorescence intensity in the EGFP channel was determined. For each condition, at least 10 cells and at least 28 SGs were analyzed. For display of fluorescence intensity of FUS in SGs, measured fluorescence values were log transformed to achieve a more balanced spread. Statistical analyses were performed in GraphPad Prism 5.

Quantification of filter-binding assays

Membranes from filter-binding assays were scanned by a FujiFilm FLA-3000 imaging machine. Quantification of signal intensities was carried out using the Dot Blot Analyzer macro within the ImageJ software. For binding experiments, the raw intensities of the individual dots on the nitrocellulose membrane were normalized against the raw intensity measured for the highest FUS concentration. For outcompetition experiments, a ratio of the intensity on the nitrocellulose membrane versus the intensity on nitrocellulose and nylon membrane was determined. The obtained relative intensities were plotted against the protein concentration and fitted using the non-linear curve-fitting tool in Origin software.

FRAP analysis

Intensities of bleached areas were corrected both for bleaching due to imaging over time and background noise. The corresponding calculations were performed with the FIJI/ImageJ macro "TimeSeries Analyzer" by calculating the fluorescence intensity over time (I(t)) as follows:

$$I(t) = [ROI1(t) - ROI3(t)] / [ROI2(t) - ROI3(t)]$$

with ROI1 giving the averaged gray values of the bleached area, and ROI2 corresponds to the averaged gray values of the total droplet. ROI3 corresponded to the averaged background values. Obtained values were further normalized to the initial fluorescence by dividing I(t) by the mean gray value of the initial 4 time steps before bleaching $< I(1\text{-}4) >$.

Densitometry measurements

To determine the solubility of FUS by sedimentation analysis of TEV-cleaved MBP-FUS, densitometry measurements of band intensities after Sypro-Ruby staining or FUS immunoblotting of supernatant and pellet fractions, respectively, were performed using standard plugins in the ImageJ software.

Cell

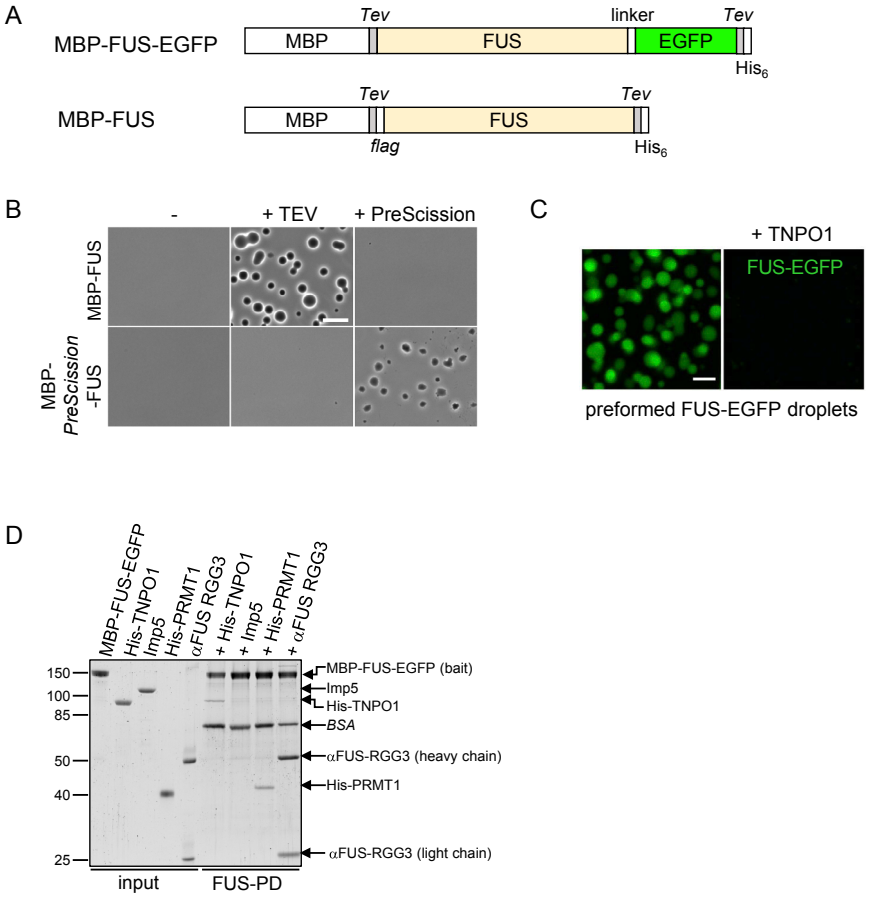

Figure S1. TNPO1 Inhibits and Reverses Phase Separation of FUS *In Vitro*, Related to Figure 1

(A) Scheme of MBP-FUS-EGFP and MBP-FUS. Human FUS was N-terminally tagged with maltose binding protein (MBP), which keeps FUS soluble, and C-terminally with a His_6-tag. In MBP-FUS-EGFP, FUS and the EGFP-His_6 tag are separated by a 13 amino acid linker in order to preserve functionality of the PY-NLS. To initiate phase separation, the MBP- and His_6-tags are cleaved off using TEV protease, which cleaves at the indicated sites *(Tev)*.

(B) Phase contrast microscopy demonstrates that TEV induces droplet formation when added to MBP-FUS harboring a *Tev* cleavage site, but does not cause phase separation of MBP-*Precission*-FUS. Scale bar, 10 μm.

(C) Preformed FUS-EGFP droplets (6 μM) were mixed with equimolar amounts of TNPO1. A highly concentrated TNPO1 stock (140 μM) in droplet buffer was used, to avoid changes in FUS-EGFP droplet concentration and buffer conditions. Droplets dissolve upon addition of TNPO1. Images were acquired by confocal fluorescence microscopy. Scale bar, 5 μm.

(D) Pulldown (PD) testing for the direct interaction of MBP-FUS-EGFP, immobilized on amylose beads, with various proteins visualized by SyproRuby staining. Input and PD correspond to 5% or 30%, respectively. Molecular weight markers (in kDa) are indicated on the left.

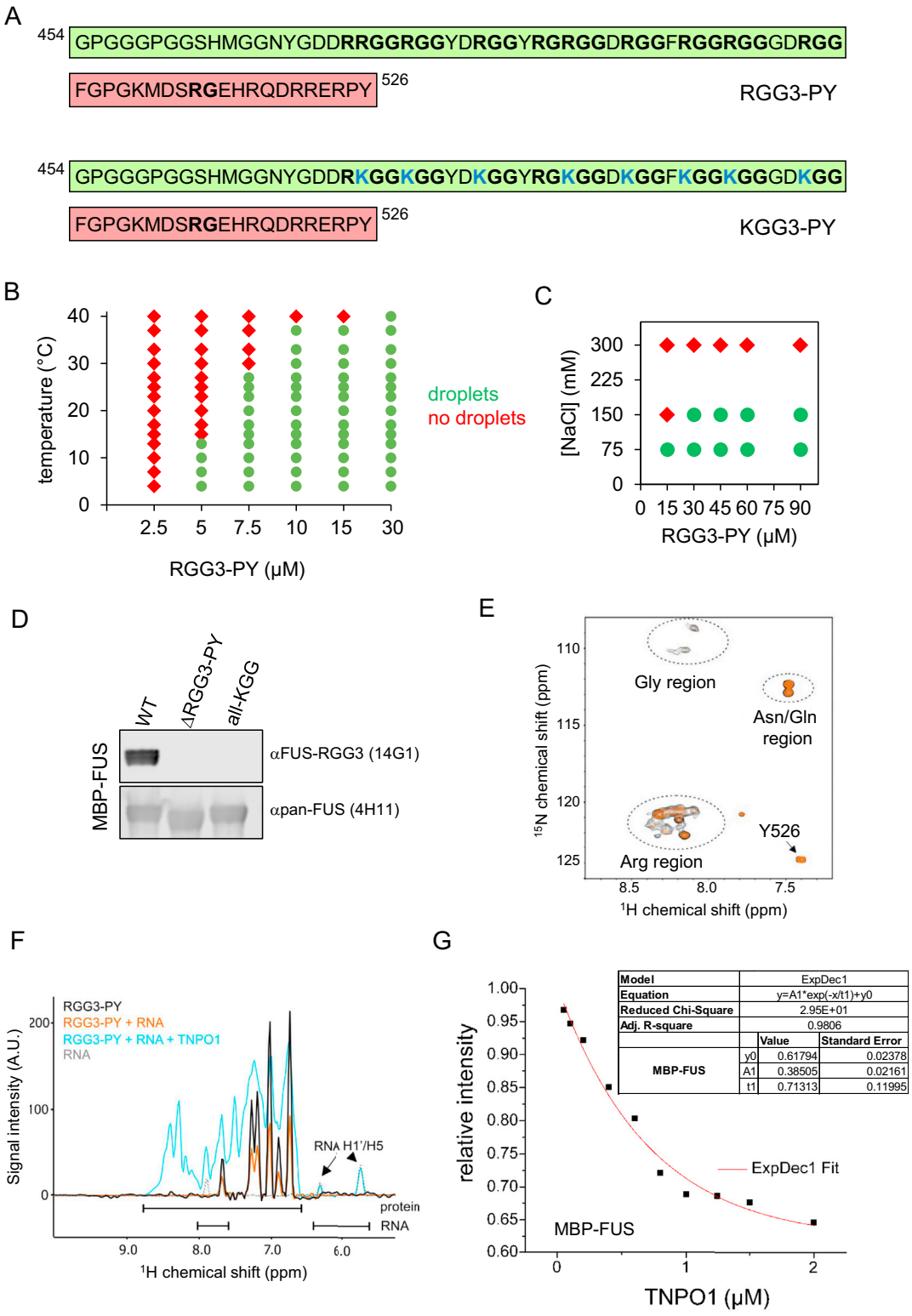

Figure S2. Phase Separation Properties of RGG3-PY Domain, Related to Figure 3

(A) Amino acid sequence of RGG3-PY domain (RGG3 in light green, PY-NLS in light red) showing that it is highly enriched in RGG/RG motifs (bold). In the KGG3-PY mutant, all arginines in RGG motifs are replaced by lysine (highlighted in blue).

(legend continued on next page)

(B and C) Phase diagram of RGG3-PY at different protein concentrations as a function of temperature (B) or salt concentration (C), obtained by scoring for the presence of droplets (green circles) or absence of droplets (red diamonds).

(D) Western blots with an antibody specific for FUS-RGG3 (14G1) demonstrating that signal is lost in mutant MBP-FUS proteins (FUS-ΔRGG3-PY and FUS-all-KGG). Equal loading was demonstrated using an anti-FUS antibody binding N-terminally of the RGG3-domain (4H11).

(E) NMR data demonstrating RNA-mediated phase separation of RGG3-PY. ^{1}H-^{15}N SOFAST-HMQC spectrum of ^{15}N-labeled RGG3-PY without (black) or with 0.2 stoichiometric equivalents of $(UG)_{10}$ RNA (orange). Spectra were recorded with an interscan delay of 1.0 s, spectral widths of 16/32 ppm, centered at 4.7/115.0 ppm in $^{1}H/^{15}N$, with 512 and 128 complex data points, respectively, and 8 scans per increment.

(F) NMR data demonstrating that TNPO1 displaces RNA from RGG3-PY. Overlay of ^{1}H NMR spectra of ^{15}N-labeled RGG3-PY (black), in presence of 0.2 stoichiometric equivalents of RNA (orange), and with an additional stoichiometric equivalent of TNPO1 (light blue), respectively. The reference ^{1}H NMR spectra of RNA at the same concentration of 20 μM is shown in gray (dotted line). Protein concentrations were 100 μM. Spectra were recorded with an interscan delay of 1.0 s, spectral widths of 20 ppm, centered at 4.7 ppm in ^{1}H, with 512 complex data points and 256 scans.

(G) Representative plot of relative signal intensities from filter binding assays shown in Figure 3F. The relative intensity was plotted against the respective TNPO1 concentration. Curves were fitted using the exponential decay fitting algorithm (in Origin software). Table summarizes the amplitude and decay factor of three independent experiments.

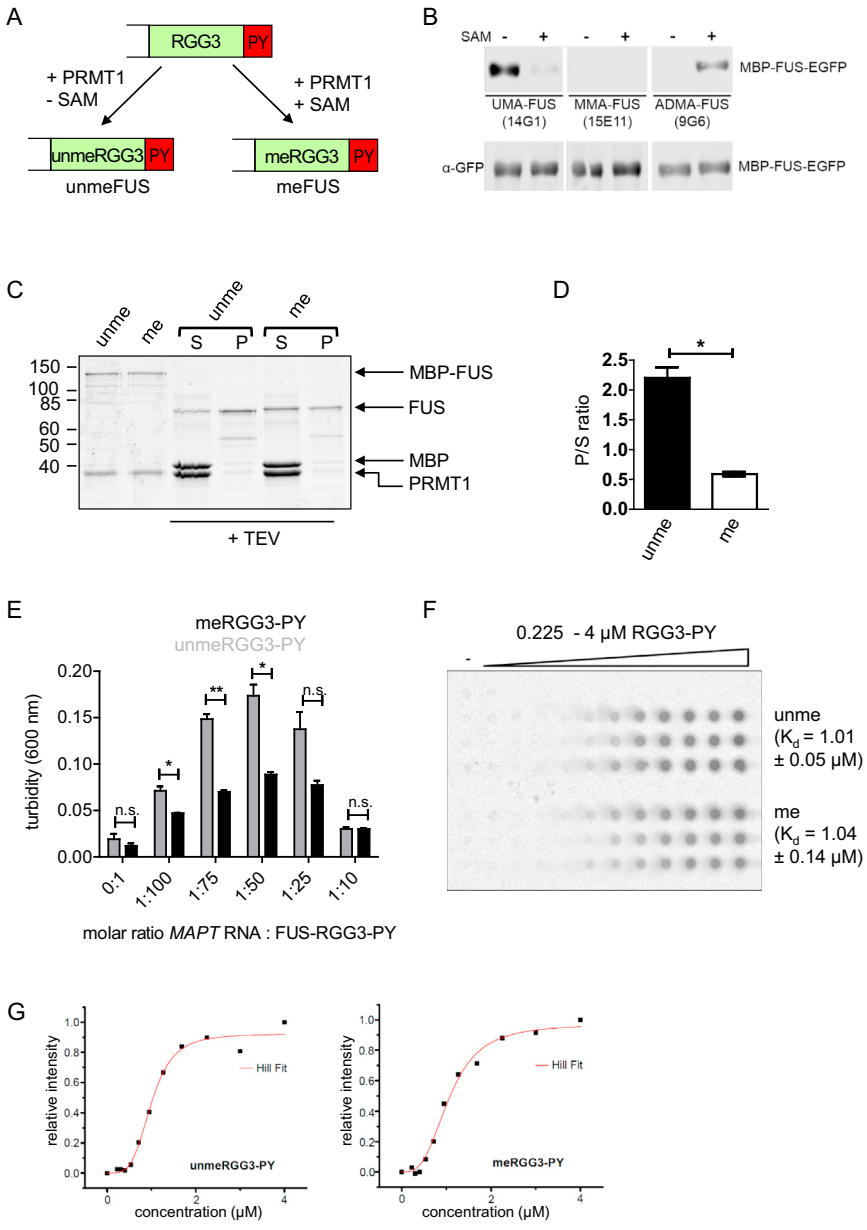

Figure S3. Comparison of Phase Separation Properties of *In Vitro* Methylated versus Unmethylated FUS, Related to Figure 4

(A) Scheme of *in vitro* methylation. Purified FUS proteins were *in vitro* methylated with recombinant PRMT1 as methylating enzyme and the methyl group donor *S*-adenosylmethionine (+SAM). A sample with PRMT1 and without SAM (-SAM) served as unmethylated control.

(B) Methylation was confirmed by immunoblotting with antibodies specific for the FUS-RGG3 domain containing unmethylated arginines (UMA-FUS, 14G1), monomethylated arginines (MMA-FUS, 15E11) and asymmetrically dimethylated arginines (ADMA-FUS, 9G6), respectively. Here, immunoblots are shown for MBP-FUS-EGFP, immunoblotting with a EGFP-specific antibody demonstrates equal loading. Immunoblots for MBP-FUS and RGG3-PY demonstrated similar methylation efficiencies (data not shown).

(C) Precipitation of unmethylated (unme) and methylated (me) FUS after cleavage of MBP-FUS by TEV protease. Equal volumes of supernatant (S) and pellet (P) fractions were analyzed by SDS-PAGE/Sypro-Ruby stain. Molecular weight markers (in kDa) are indicated on the left. As indicated in the scheme in (A), PRMT1 (but not SAM) was present in both protein samples to ensure comparability. A quantification of the ratio P/S is shown in (D). Values represent means ± SEM from three independent experiments.*$p < 0.05$ by paired t test.

(E) Turbidity measurements to quantify phase separation of the unmethylated (unme) or methylated (me) RGG3-PY domain (30 μM) in presence of different amounts of *in vitro* transcribed *MAPT* RNA. Values represent means ± SEM (n = 3). **$p < 0.01$ and *$p < 0.05$ by paired t test.

(F) Representative images of nitrocellulose membranes from filter binding assay with unmethylated (unme) and methylated (me) RGG3-PY and radioactively labeled *ASH1* E3-51 RNA.

(G) Equilibrium dissociation constants (K_d) were determined using Hill fitting algorithm (n = 6).

See also Table S2.

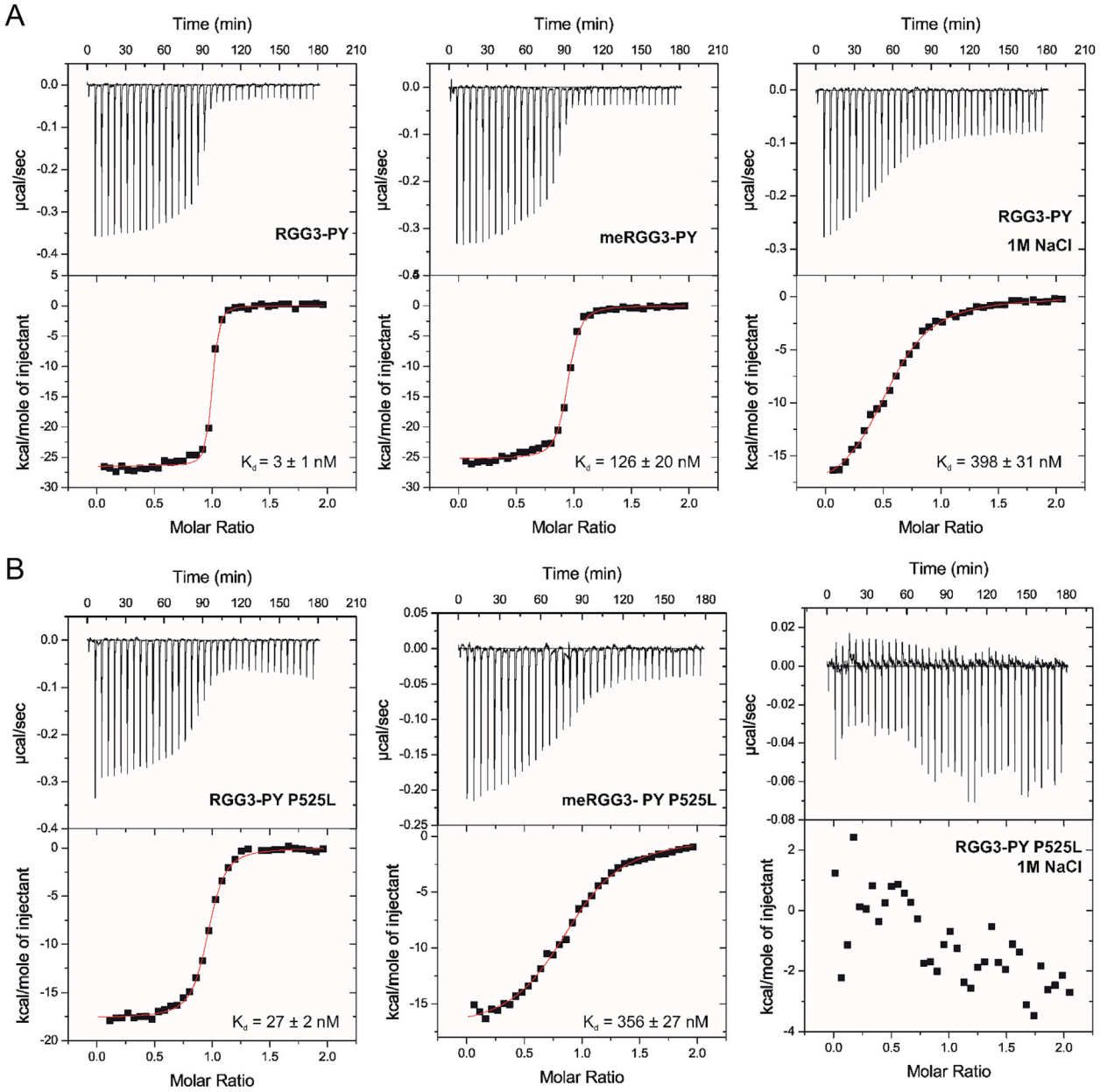

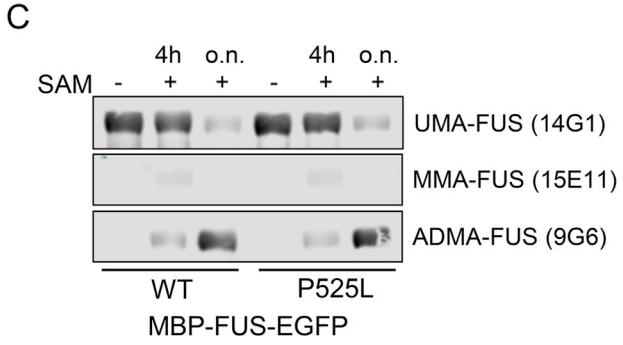

(legend on next page)

Figure S4. Affinities of Unmethylated and Methylated RGG3-PY (WT and P525L) for TNPO1 and Methylation Status of MBP-FUS-EGFP (WT and P525L), Related to Figure 5

(A) Titration of either 45 μM of RGG3-PY, meRGG3-PY or RGG3-PY (1M NaCl) into a solution containing 5 μM of TNPO1 (left, middle and right panel, respectively). The resulting K_ds are indicated, also see Table S1. The reported errors correspond to the SD of the fit.

(B) Titration of either 45 μM of RGG3-PY P525L, meRGG3-PY P525L or RGG3-PY P525L (1M NaCl) into a solution containing 4 μM of TNPO1 (left, middle and right panel, respectively). The resulting K_ds are indicated, also see Table S1. The reported errors correspond to the SD of the fit.

(C) Recombinant MBP-FUS-EGFP was *in vitro* methylated with recombinant PRMT1 and the methyl group donor *S*-adenosylmethionine (SAM +). A sample with PRMT1 and without SAM (–) served as unmethylated control. Similar degree of methylation for MBP-FUS-EGFP WT and P525L was confirmed by immunoblotting with antibodies specific for the FUS-RGG3 domain containing unmethylated arginines (UMA-FUS, 14G1), monomethylated arginines (MMA-FUS, 15E11) and asymmetrically dimethylated arginines (ADMA-FUS, 9G6), respectively. Samples from overnight (o.n.) incubation were used in experiments displayed in Figures 5A–5D.